Advances in SPECT camera software and hardware: Currently available and new on the horizon

E. Gordon DePuey, MD

INTRODUCTION

A long-standing limitation of radionuclide myocardial perfusion SPECT is its relatively lengthy acquisition time, as compared to stress echocardiography and cardiac CT. The American Society of Nuclear Cardiology (ASNC) and the Intersocietal Commission for the Accreditation of Nuclear Medicine Laboratories (ICANL) have rightfully insisted that acquisition times not be decreased below those set forth in the ASNC Guidelines so that adequate image counting statistics are maintained, thereby maintaining test sensitivity and minimizing artifacts associated with low count density studies. New software methods and new innovative hardware described below, however, now allow for significantly shortened SPECT acquisition times without a decrease in image quality.

More recently, the media, the public, and the medical community have drawn attention to patient radiation exposure associated with radiographic, nuclear medicine, and nuclear cardiology procedures and the potential-associated patient risk.[1,2] The radiology and nuclear imaging communities have responded rapidly and definitively by implementing a variety of guidelines to decrease patient radiation exposure and to avoid exposure in higher risk patient populations: Image Gently, Image Wisely, Choosing Wisely, and the ASNC Patient-Centered Imaging Guidelines,[3] among others. ASNC has set a goal to decrease patient radiation exposure associated with myocardial perfusion SPECT to <9 mSv per entire study in 50% of patients by 2014.[4] The new software and hardware methods described below will help us achieve this goal by providing the ability to maintain or improve SPECT image quality with the lower image counting statistics associated with significantly decreased injected radiopharmaceutical doses.

From the St. Luke s Hospital, Nuclear Medicine, New York, NY.
Reprint requests: E. Gordon DePuey, MD, St. Luke's Hospital, Nuclear Medicine, New York, NY; *edepuey@chpnet.org*.
J Nucl Cardiol 2012;19:551–81.
1071-3581/$34.00

doi:10.1007/s12350-012-9544-7

There have been several comprehensive reviews and editorials published highlighting innovations in cardiac SPECT hardware and software.[5-9] I hope the present review will serve to reinforce the importance and clinical significance of these technical advancements. Of note, advancements in hybrid SPECT/CT imaging are not covered in the present review.

TECHNICAL ADVANCEMENTS

New Software Methods

New SPECT reconstructions software methods have preserved or improved SPECT image quality despite lower count statistics. Consequently, SPECT acquisition time may be shortened. Alternately, the injected radiopharmaceutical dose may be decreased, thereby decreasing patient radiation exposure. These methods, described below, are all now commercially available. They are available on new computer systems, and some may also be implemented on older scintillation camera systems.

Iterative reconstruction. Iterative reconstruction has been available on the nuclear medicine computer systems for over a decade, although many users have hung tenaciously to an older processing method, filtered backprojection (FBP). FBP basically suppresses high-frequency image data, thereby decreasing noise. However, in doing so the technique results in image blurring, often obscuring small perfusion abnormalities and rendering the images of both objects, i.e., the myocardium and perfusion defects indistinct. The smoother the filter, i.e., the lower the critical frequency and the higher the order, the greater the degree of image blurring and the poorer the diagnostic sensitivity in detecting perfusion abnormalities. In contrast, iterative reconstruction provides an estimated reconstruction volume from which estimated projections are derived. The estimate may be simply a uniform flood field or a more complex heuristic algorithm with an estimate of the expected configuration of the heart. Actual measured SPECT projection data are compared to the estimated

projections. Based upon the ''error'', i.e., the difference between the estimated and the measured projection information, the estimated projection is updated. This process is repeated until the estimated and the measured projections converge, resulting in an implicit recovery of resolution. The initial version of iterative reconstruction was Maximum Likelihood Expectation Maximization (MLEM), whereby individual iterations were repeated until data converged. Subsequently, with higher speed computers Ordered Subset Expectation Maximization (OSEM) has become the reconstruction method of choice, whereby data are grouped into subsets, allowing more rapid and accurate data convergence.

Myocardial perfusion SPECT images reconstructed with OSEM are of higher quality than those processed with FBP. Perfusion defects, anatomic variants such as physiologic apical thinning and prominent posterior papillary muscles, and the right ventricular myocardium are better visualized with OSEM. Likewise, image contrast is improved, thereby better defining the left ventricular endocardial borders. Although differences in FBP and OSEM may be only slight in high count density myocardial perfusion SPECT scans, in lower count density studies the improvement with OSEM is often clinically significant. Another advantage of OSEM is that the Ramp filter, inherent to FBP, is not employed, thereby minimizing the possibility of a Ramp filter artifact, i.e., an artifactual decrease in inferior left ventricular myocardial count density when intense tracer concentration is present in extracardiac structures in the *x*-plane of the left ventricle (Figure 1). However, of note, for most commercially available implementations of OSEM, a post-processing filter is employed to further improve image quality. Therefore, the Ramp filter artifact may not be eliminated entirely.

Figure 1. A This low-dose rest/high-dose stress Tc-99m sestamibi study, performed in an obese patient, was processed with FBP. Reconstructed tomograms are technically suboptimal with considerable noise and indistinct definition of the myocardial borders. Both at stress and at rest there is considerable tracer uptake in the left lobe of the liver, which lies in the *x*-plane of the inferior wall of the left ventricle. The fixed inferior perfusion defect could be secondary either to scar or a Ramp filter artifact. **B** The same study was processed with OSEM iterative reconstruction. SPECT image quality is significantly improved with less noise and sharper definition of the myocardial borders. The inferior perfusion abnormality is resolved, indicating that it was a Ramp filter artifact since OSEM does not incorporate the Ramp filter. Courtesy Gordon DePuey, St. Luke's-Roosevelt Hospital, New York, NY. ▶

Resolution recovery. The high-resolution, parallel-hole collimator used for myocardial perfusion SPECT maintains spatial resolution by accepting photons emitted from the myocardium, traveling directly perpendicular to the face of the camera and the parallel holes of the collimator. Photons emanating from voxels not directly perpendicular to the collimator hole are attenuated by the collimator's lead septa. Photons emanating from these voxels may undergo Compton scattering and may also subsequently travel perpendicular to the collimator hole. These are eliminated by the pulse height analyzer, which rejects photons losing more than 10%-15% of their initial photon energy. However, these advantages of the parallel-hole collimator are progressively compromised the more distant the voxel is from the camera face (Figure 2). The greater the distance of object from the camera face, the greater the likelihood that photons from adjacent voxels will pass through the parallel-hole collimator. Likewise, the likelihood that Compton-scattered photons will be accepted progressively increases. For these reasons spatial resolution of a voxel/object decreases with distance from the camera face. Therefore, it has always been emphasized that when a patient is positioned for myocardial perfusion SPECT, the face of the scintillation detector should be as close as possible to the patient's chest wall. Likewise, an elliptical orbit is preferable because it allows the camera head to more closely approximate the chest wall in all projections. The magnitude of this loss of resolution is directly proportional to the width of the collimator hole and inversely proportional to the hole length (Figure 3). Septal penetration of photons is another cause of decreased the resolution of a parallel-hole collimator. However, for the relatively low-energy isotopes, Tc-99m and Tl-201, used for myocardial perfusion imaging the degree of septal penetration is minimal.

This distance-dependent collimator-detector blur, dependent upon the shape of the holes, their dimensions, and the thickness of the septa for each individual collimator has a major influence on image resolution.[10,11] It is the main factor affecting the resolution and noise properties of nuclear medicine images. In reconstructed SPECT images, these effects are strongly influenced by the applied reconstruction algorithm and its parameters. Resolution recovery models the physics and geometry of the emission and detection processes. It is thereby a means to compensation for the collimator-detector response (CDR) in iterative reconstruction.[12-14] The CDR consists of four main components: intrinsic response (the system without a collimator) and the geometric, septal penetration, and septal scatter components of the collimator parameters. By including an accurate model of CDR function in an iterative SPECT reconstruction algorithm, compensation for the blurring effect may be included in the iterative reconstruction process, resulting in improved spatial resolution. For each combination of acquisition system, radiopharmaceutical, and particular acquisition protocol, the CDR

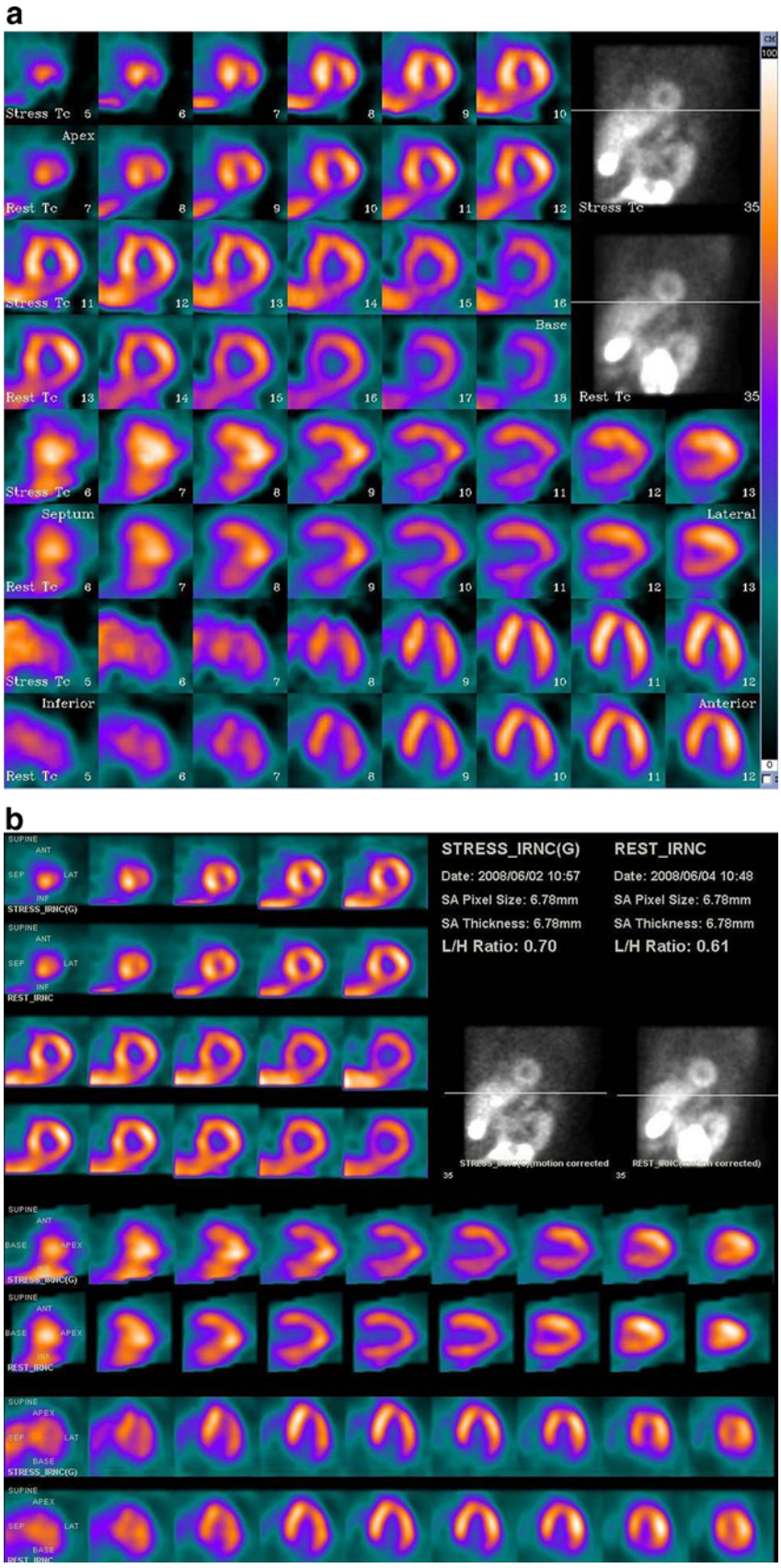
a
Stress Tc
Apex
Rest Tc
Stress Tc
Base
Rest Tc
Stress Tc
Septum
Lateral
Rest Tc
Stress Tc
Inferior
Anterior
Rest Tc
b
STRESS_IRNC(G)
Date: 2008/06/02 10:57
SA Pixel Size: 6.78mm
SA Thickness: 6.78mm
L/H Ratio: 0.70
REST_IRNC
Date: 2008/06/04 10:48
SA Pixel Size: 6.78mm
SA Thickness: 6.78mm
L/H Ratio: 0.61

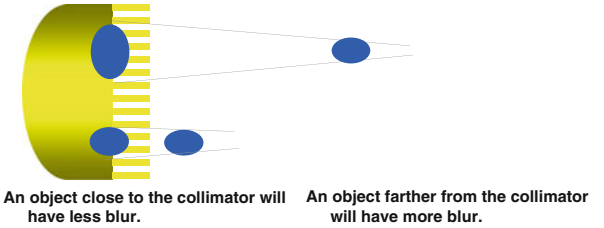

Figure 2. Depth-dependent loss of resolution. When an object is further from a parallel-hole collimator, photons emanating from the object pass through a greater number of parallel holes of the collimator, thereby blurring the object and decreasing spatial resolution. Courtesy Yossi Srour, UltraSPECT Ltd.

function provides the probability that a photon emitted from any point of the imaged object will contribute to a pixel of the resulting image. Accurate predictions of the geometric response function for various collimator designs have been derived. Specifically, during iterative reconstruction each voxel is reconstructed according to the collimator's geometry. Pixel weights are calculated analytically, taking into account the solid angles subtended by the collimator between each detector pixel and each body voxel. This is accomplished by knowing the CDR for each particular scintillation camera/collimator system.

To implement resolution recovery acquisition parameters including the center-of-rotation and the collimator-to-voxel distances for every projection view acquired must be known. Additionally, in order to apply pixel weighting appropriately to the image matrix, which includes the heart and surrounding body structures, the distance from the detector to the patient's body must be determined. Newer cameras automatically provide this distance in the acquired parameters for each angular position. However, for cameras that do not provide this distance automatically from the acquisition parameters, a simple segmentation algorithm may be applied to the projections to estimate the detector-to-body distance.

One resolution recovery method, incorporated into Wide Beam Reconstruction® (WBR®) (UltraSPECT, Ltd.), models the CDR and the physics and geometry of the emission and detection processes.[15] As described above, the shape of the holes, their dimensions, and the thickness of the septa for each individual collimator have a major influence on image resolution. Therefore, during iterative reconstruction data are modified in each reconstructed voxel according to the collimator's geometry. Pixel weights are calculated analytically, taking into account the solid angles subtended by the collimator between each detector pixel and each body voxel (Figure 4). With knowledge of various scintillation detector systems and collimators, this resolution

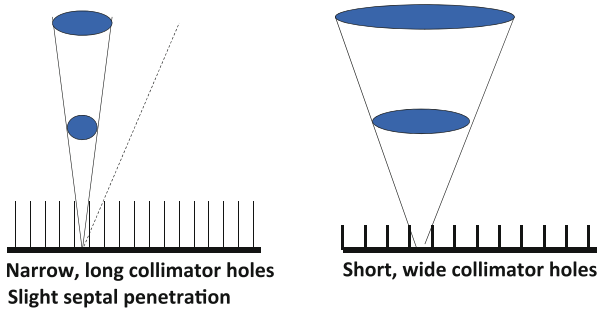

Figure 3. Loss of resolution with the depth from the parallel-hole collimator depends upon the collimator hole characteristics. For a collimator with narrow, long holes (*left*) the loss of resolution with depth is less than that of a collimator with short, wide holes (*right*). Septal penetration of photons also contributes to image blurring (*left*), although this factor is minor for low-energy isotopes such as Tc-99m.

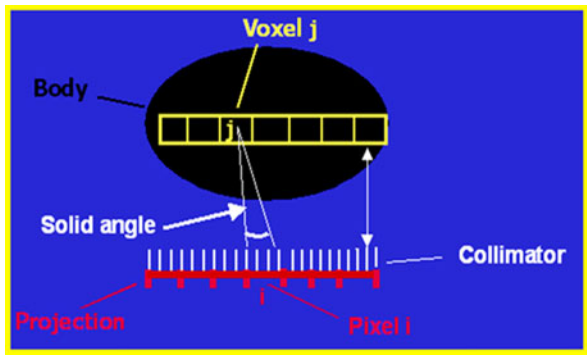

Figure 4. During iterative reconstruction data are modified in each reconstructed voxel according to the collimator's geometry. Pixel weights are calculated analytically, taking into account the solid angles subtended by the collimator between each detector pixel and each body voxel. Also, in order to apply pixel weighting appropriately to the image matrix, the distance from the detector to the patient's body is accounted for.

recovery method can be implemented on both newer and older cameras.

Therefore, resolution recovery yields images of improved spatial resolution and with less noise as compared to conventional techniques.[15] Clinical images of lower count density acquired with resolution recovery have been demonstrated to be equivalent or superior to those acquired with conventional SPECT imaging, allowing for reduced SPECT acquisition time or reduced injected radiopharmaceutical dose (see below).

Noise compensation. Nuclear imaging data are inherently noisy due to relatively poor counting statistics. Low count density myocardial perfusion SPECT images are characterized by noise, which has similar or higher magnitude compared to the high-frequency portion of the true myocardial data. As

described above, FBP eliminates high-frequency data, thereby ''smoothing'' (i.e., blurring) the image. This filtering results in decreased image contrast, decreased spatial resolution, and potentially decreased diagnostic sensitivity in detecting perfusion and regional wall motion abnormalities. In contrast, with noise compensation methods signal-to-noise values are determined by the resolution and smoothness desired in the final cardiac SPECT image. High-frequency components of the image are suppressed while resolution is maintained (Figure 5).

One noise compensation technique, WBR® (UltraSPECT, Ltd.), suppresses noise and enhances the signal-to-noise ratio (SNR) by modeling the statistical characteristics of the emission process and of the detected data.[16] It accounts for the Poisson distribution of the emission data, as well as for the noise in the acquired data. To preserve or even enhance the SNR, WBR® regularizes the likelihood objective function by adding a Gaussian component. Higher weight to the Gaussian component results in suppressed high-frequency components present in the projections, due to its fast vanishing tail. Higher weighting of the Poisson component results in recovery of high-frequency signal, or enhancement of noise if no appropriate weight is given. The balance between the two is determined adaptively and automatically according to the data analysis and desired smoothness. The reconstruction is iterative and automatic with all noise compensation parameters selected automatically and with no post-filter applied. The smoothness of the image is guided by the application's target SNR without applying filters during or post-reconstruction (Figure 6). For the WBR® method, incorporating iterative reconstruction, resolution recovery, and noise compensation, the spatial resolution (FWHM) for three line sources with scatter was reported to be 5.1 mm, as compared to 10.2 mm (coefficient of variation = 3.7% for both) for standard FBP processing. Contrast resolution from Data Spectrum phantom experiments (with scatter) was 0.67 compared to 0.53 for FBP (coefficient of variation = 12% for both).[15]

Of note, resolution recovery algorithms themselves may result in accentuation of noise in reduced-time acquired projections. This has a detrimental effect on image quality. One method, adopted in the General Electric Evolution® software suppresses the impact of noise by incorporating a Maximum A Posteriori (MAP) Algorithm.[17] The scheme used is a modified one step late (OSL) algorithm using a Green prior optimized for each clinical protocol, and for gated and attenuation corrected image.[18] The last iteration is performed using a Median root prior.[19] This scheme was found to give an image of equal or superior quality on clinical studies and on physical phantom data.[20]

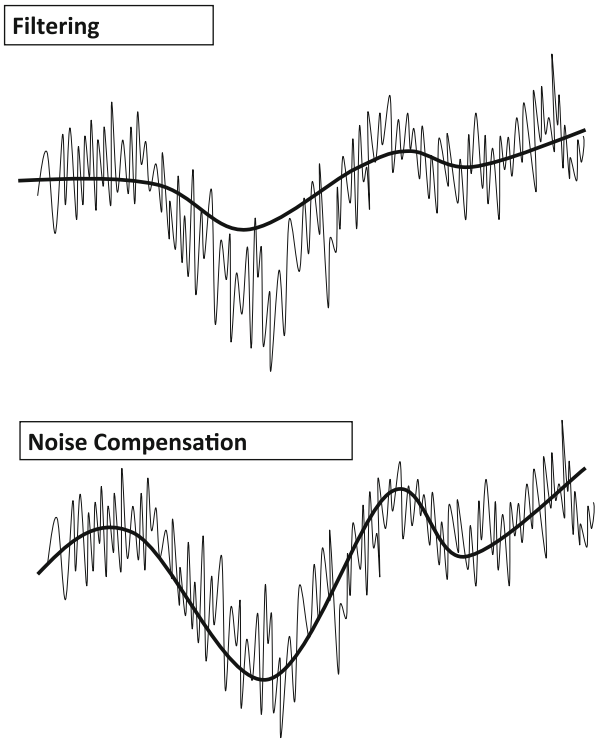

Figure 5. Comparison of the effects of filtering and noise compensation on a myocardial perfusion count-rate profile. A representative profile across an object demonstrates considerable high-frequency noise. Filtering, i.e., smoothing, the data (*top*) decreases noise, but at the same time considerably decreases image resolution and contrast. On the other hand, with noise compensation (*bottom*) signal-to-noise values are determined by the resolution and smoothness desired in the final SPECT image. High-frequency components of the image are suppressed while resolution and contrast are maintained. Concept courtesy of Ernest Garcia, Emory University, Atlanta, GA.

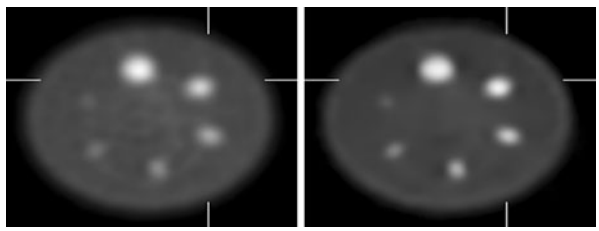

Figure 6. Tomographic slice through the Jaszczak phantom containing low-level Tc-99m background tracer concentration and spheres of various diameters containing higher level activity. With FBP reconstruction (*left*) there is moderate noise in the background area, and the edges of the spheres are blurred. With WBR® reconstruction (*right*), incorporating resolution recovery and noise compensation, background noise is suppressed, and resolution and contrast of the spheres are increased[15].

Vendors of conventional SPECT cameras as well as the new, innovative cameras described below have all adopted advanced software processing methods, including iterative reconstruction, resolution recovery, and some type of noise compensation. These software packages include Astonish®, Phillips; Shine®, Segami; Evolution®, General Electric Medical Systems; 3-D Flash®, Siemens Medical Solutions; n-SPEED®, Digirad, Inc.; and proprietary software developed by General Electric for the Discovery 530c camera and by Spectrum Dynamics for the D-SPECT camera. Users should be aware that these software programs each use different reconstruction algorithms, so results are by no means identical.

Pre-determined SPECT acquisition times to obtain optimal counts. The introduction of dual-head cameras more than a decade ago allowed us to halve acquisition times as compared to acquisition times for studies performed on older single-head cameras. Since their introduction, however, cardiac SPECT protocols have been rather rigid with regards to image acquisition times. For larger patients with soft tissue attenuation resulting in low count density studies ''weight-based dosing'' was recommended to increase cardiac SPECT counting statistics. However, by increasing the radiopharmaceutical dose, patient radiation exposure is likewise increased. As an alternative to increasing the radiopharmaceutical dose, it is possible to increase SPECT acquisition time in cooperative patients. Newer ''smart'' cameras allow optimal SPECT acquisition times to be predetermined in such patients. For example, TruACQ® software available on the Digirad Cardius® camera determines the count rate from regions of interest manually placed over the heart on each of its three detectors. An acquisition time is then pre-determined which will result in 22,000 counts in the heart (in the LAO projection) at stress and 10,000 counts at rest. The camera operator can accept or reject this suggested acquisition time, depending upon the patient's tolerance. By this means optimal counting statistics can be obtained in larger patients without increasing the radiopharmaceutical dose.

Phase analysis. Innovative software has been developed to measure left ventricular systolic dyssynchrony using phase analysis of gated myocardial perfusion SPECT.[21] Increasing myocardial counts during ventricular systole correlates with regional left ventricular wall thickening and may be used to assess the pattern of systolic contraction. Data from the entire myocardium are used to generate a phase distribution map that may be displayed as a histogram or polar map. By means of a sampling theorem, temporal changes in left ventricular myocardial contraction can be assessed using only 8 frames per cardiac cycle. This method provides temporal resolution equivalent only 1/64th of the cardiac cycle. Left ventricular dyssynchrony assessed by this technique in 75 heart failure patients was compared to echocardiographic tissue Doppler imaging and was found to correlate well ($r = 0.89$, $P < .0001$).[22] It has been reported that left ventricular dyssynchrony measured by this method is useful to predict which patients will respond to cardiac resynchronization therapy (CRT).[23] Using a phase histogram bandwidth of approximately 140°, this method demonstrated a sensitivity of 70% and specificity of 74% in predicting patient response to CRT. Although this radionuclide method is quite promising, there have been parallel advancements in echocardiography, magnetic resonance imaging, and cardiac computed tomography in assessing left ventricular dyssynchrony and patient response to CRT.[24]

Hardware Developments

Optimized detector geometry and focused collimation.

Dedicated sodium iodide detector cardiac SPECT cameras. Well over a decade ago scintillation camera designs were modified to better perform dedicated cardiac imaging. Phillips introduced the CardioMD® camera with two 90°-angled detectors that could be positioned close to the patient's chest wall to optimize detector geometry and minimize detector-to-voxel blurring. The open gantry design was patient-friendly, even for most claustrophobic patients. The design was compact, allowing the small footprint camera to fit easily into an $8' \times 10'$ room. General Electric introduced the Optima® camera, with similar advantageous characteristics. Both of these cameras could be equipped with rod-source attenuation correction (AC). Subsequently, dedicated cardiac SPECT cameras were introduced to accommodate larger patients. One example is the General Electric Ventri® camera with two independent detectors positioned in a 90° geometry, mounted on a ring gantry. Patients are comfortably positioned on an imaging palate, sturdy enough to accommodate the patients up to 440 pounds, with supports engineered to relieve pressure on the arms, knees, low back, and neck. The palate slides into the ring detector of the gantry, and the detectors are then positioned close to the chest wall in an optimal geometry for cardiac SPECT. The advantages of such dedicated cardiac SPECT cameras are considerable. However, for a general Nuclear Medicine laboratory they lack the flexibility to perform other non-cardiac scans.

Dedicated upright and semi-reclining cardiac SPECT cameras. Patients are positioned upright with the Digirad camera and semi-upright/semi-reclining with the Siemens C-Cam® camera and the Data

Spectrum D-SPECT® camera. Each of these cameras has a small footprint and is designed for patient comfort. Upright or semi-reclining positioning allows the diaphragm to move inferiorly, thereby decreasing diaphragmatic attenuation and Compton scatter from sub-diaphragmatic structures. A second advantage of upright or semi-upright positioning is that pendulous breasts are less likely to assume different positions in the stress and the rest SPECT acquisitions, a problem occasionally encountered with supine SPECT, resulting in ''shifting'' breast artifacts mimicking ischemia. Photon attenuation artifacts involving the inferior wall due to an overlying pendulous left breast, however, are more likely with upright and semi-upright/reclining patient positioning. Patient motion was problematic for the long acquisition times required for earlier single-head versions of the Digirad upright camera. However, in the most recent release of the multi-head camera shorter acquisition times combined with Velcro straps/binders around the patient's waist and chest effectively minimize motion, particularly in the *Y*- and *Z*-directions.

Cardiocentric SPECT. Conventional myocardial perfusion SPECT performed with a single- or dual-head scintillation camera, as described above, employs a body-centered orbit. However, SPECT images acquired with such a 180° body-centered orbit may have significant erroneous inhomogeneity and may overestimate defect size, particularly when the target object is off the center of the orbit, as is commonly the case in clinical cardiac imaging.[25] Although, elliptical body-centered orbits minimize the distance between the heart and the detector in all tomographic projections, thereby minimizing distance-dependent image blurring and scatter, SPECT artifacts, particularly those at the left ventricular apex, may be more severe in scans using elliptical orbits than in those from circular acquisitions.[26]

Newer camera designs incorporate ''cardiocentric'' SPECT orbits. Detector design and/or translation of either the camera heads or the patient before or during SPECT acquisition allow the heart to remain in the center of the field-of-view. For example, the Digirad Cardius® camera uses a triple-head geometry. The patient sits on a translating chair. Immediately prior to the SPECT acquisition the patient's heart is positioned in the center of the field-of-view of each detector. The detector heads are pushed in as close as possible to the patient's chest to optimize image quality. For the SPECT acquisition the chair rotates 67.5°, allowing the triple-head camera to acquire data in a 202.5° cardiocentric orbit. This triple-head configuration used in combination with 3-dimensional OSEM nSPEED® reconstruction enables emission scans to be performed up to four times faster than with conventional dual-head SPECT systems.[27] Image quality is improved as compared to body-centered orbits, and the severity of artifacts is reduced[27] (Figure 7). New collimator designs and other new cameras, described below, including the Spectrum Dynamics D-SPECT® camera and the General Electric Discovery 530c® camera, also incorporate cardiocentric SPECT.

Cardio-focused collimation. A cardio-focused collimator, IQ SPECT®, has been developed by Siemens Medical Solutions to improve the efficiency of myocardial perfusion imaging using conventional, large field-of-view SPECT and SPECT/CT systems (Figure 8).[28,29] This variable-focus collimator is designed to magnify the region of the myocardium and its immediate surroundings by means of converging collimation, while keeping the entire torso in the field-of-view by morphing the collimator holes to a near parallel-hole geometry at the edges of the collimator, thereby avoiding truncation. There are 48,000 hexagonal holes, each 1.9 mm in diameter and 40 mm in length. Spatial resolution progressively increases from the face of a camera to the cardiac ''sweet-spot'' at 28 cm. The scan orbit is cardiocentric, 28 cm from the center of rotation, as determined by the operator, so that the heart is maintained in the region of highest magnification throughout the scan. A scanning arc of 104° with 6° angular steps is used for each of the two 90°-angled camera heads.

Since the collimator has a response that is not only distance-dependent but also variable across the face of the collimator, it is crucial to accurately model both the

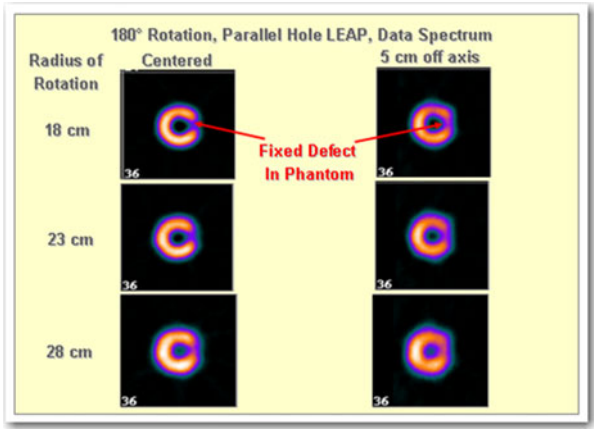

Figure 7. A data spectrum phantom, filled with Tc-99m, with a full-thickness insert in the posterior wall was imaged with a 180° cardio-centric orbit (*left*) and again with an off-center orbit (*right*), simulating a body-centered orbit. The radius of rotation of the orbit was progressively increased from 18 to 23 to 28 cm. The posterior defect is better resolved using a cardiocentric orbit, particularly with a smaller camera radius of rotation. Courtesy, Richard Conwell and Chuanyong Bai, Digirad Inc.

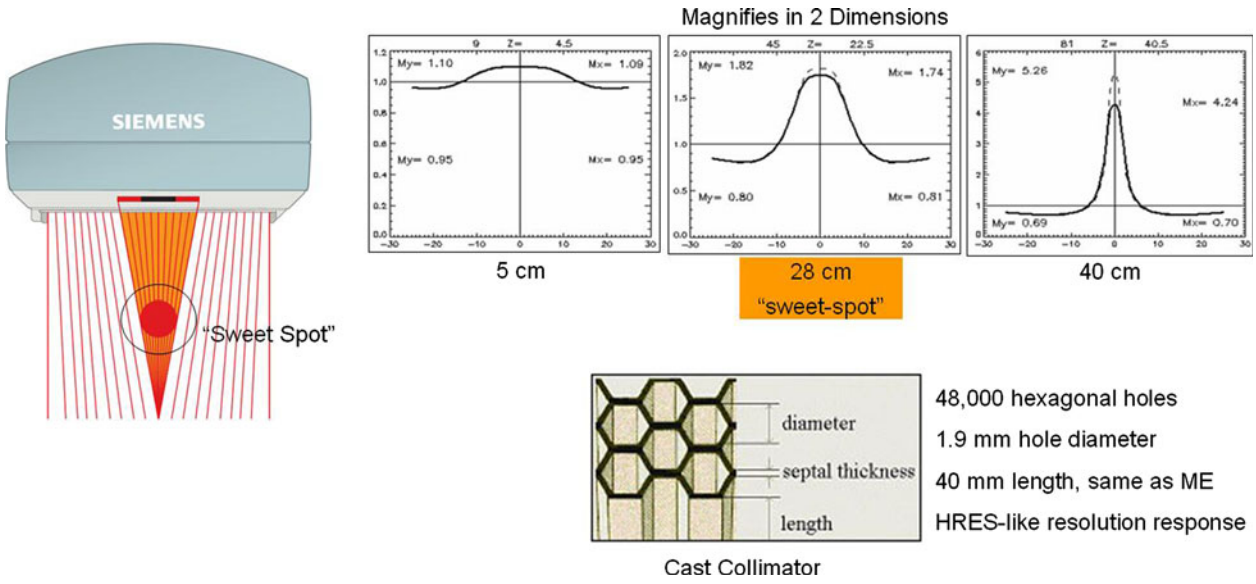

Figure 8. Diagram of the IQ SPECT® variable-focus collimator, demonstrating magnification of the region of the myocardium and its immediate surroundings by means of converging collimation, while keeping the entire torso in the field-of-view by morphing the collimator holes to a near-parallel-hole geometry at the edges of the collimator. Spatial resolution increases with depth from the central area of the collimator surface.[30] Courtesy Siemens Medical Solutions.

magnification and the point-response function of the collimator. Variable magnification results from the changing direction of each borehole with respect to the collimator surface normal vector, while the point response function depends on the finite size of the bore holes. Therefore, an advanced reconstruction engine based on a conjugate-gradient algorithm with ordered subsets that includes in the system matrix the view-angle dependent gantry deflections, a vector map of the collimator hole angles, and the system's point response function, is used for cardiac SPECT reconstruction. Based upon phantom experiments, as compared to a conventional low-energy high-resolution collimator, this novel cardio-focused collimator increases target sensitivity at 28 cm by a factor of $\geq$4 while maintaining comparable reconstructed resolution. The average resolution (FWHM) is 6.97 mm in the *x*-plane and 6.91 mm in the *y*-plane.[30] Therefore, with this novel collimator scan times, patient dose, or a combination thereof may be reduced by a factor of four while maintaining acceptable spatial resolution.[31]

Arc detector geometry with rotating slit-hole collimation. The CardiArc® scanner, dedicated to performing myocardial perfusion SPECT scans, manufactured by CardiArc Inc., uses a stationary curved camera head subtending a 180° angle, which is positioned centered over the patient's precordium.[6] The curved detector is composed of three adjacent curved sodium iodide crystals. Scintillation events are detected by an array of photomultiplier tubes mounted on the back of these detectors. Vertical collimation is achieved using a unique curved lead sheet with six vertical slits that rotates back-and-forth during acquisition to obtain data over the 180° imaging arc (Figure 9). The movement of these six slits is synchronized electronically with the six areas of the crystal that are imaging the photons passing through the slits. Horizontal collimation is accomplished by a series of thin lead sheets that are stacked vertically, with the gaps between the slits defining the hole apertures. By means of this ''slit-hole'' method, collimation is focused at the depth of the heart, thereby increasing sensitivity and resolution. Counting statistics comparable to those obtained with a conventional parallel-hole collimator in 21 minutes can be achieved in only approximately 5 minutes with the CardiArc® scanner. The FWHM is 3.65 mm at a depth of 87 mm and 6.01 mm at 176 mm. To date, no clinical validation of this system has been published.

Multiple scanning parallel-hole collimators. The D-SPECT® camera, manufactured by Spectrum Dynamics incorporates nine pixilated cadmium zinc telluride (CZT) crystal detector columns situated vertically, spanning an L-shaped 90° geometry (Figure 10). The patient is positioned semi-reclining, in a posture similar to that assumed a dentist's chair. The L-shaped detector is positioned over the patient's chest, centered over the left precordium. Each of the CZT detectors is fitted with a square-hole tungsten collimator with an inherent high transmission efficiency. The collimator holes are 21.7 mm in length and measure 2.26 mm on

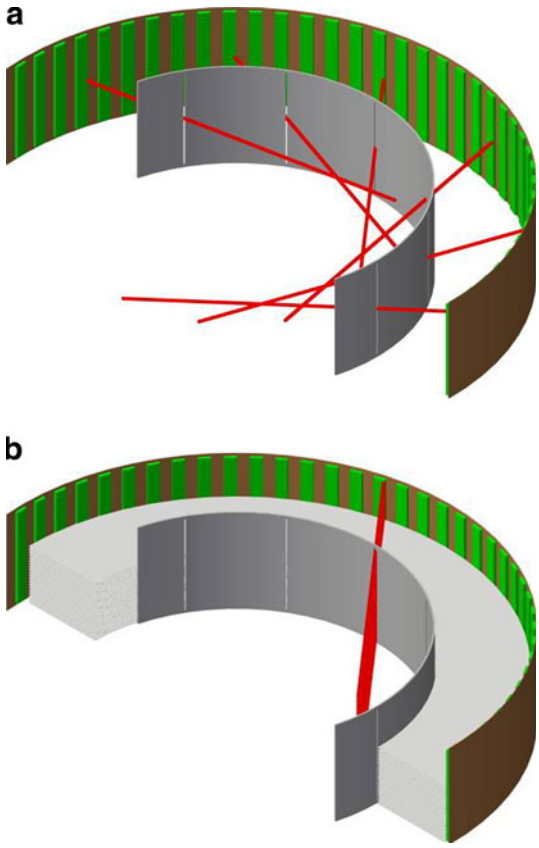

Figure 9. With the Cardiac Arc® Camera vertical collimation is achieved using a unique curved lead sheet with six vertical slits that rotates back-and-forth during acquisition to obtain data over the 180° imaging arc (**A**). Horizontal collimation is accomplished by a series of thin lead sheets that are stacked vertically (**B**). Courtesy Jack Juni, CardiArc Inc.

each side of each square hole.[32] These holes are shorter and wider than those used in conventional NaI detector low-energy, high-resolution collimators, which are typically 45-mm long and 1.6-mm wide. Consequently, the solid angle for acceptance of incident photons for the D-SPECT® collimator is more than 8 times that of the standard low-energy high-resolution lead parallel-hole SPECT collimator.

Emission data are first sampled by obtaining a 15-second scout scan to allow the nine detectors to identify the location of the heart. Each collimated detector column rotates and translates independently a maximum of 110°, allowing voxels to be viewed from hundreds of different viewing angles. Data are acquired in list mode, allowing physiologic markers such as the electrocardiographic R wave, to be recorded simultaneously. A sinogram is reconstructed and the location of the heart is derived, thereby setting the limits of the detectors' fanning motion for a subsequent diagnostic scan. The diagnostic scan, typically a 4-minute acquisition, is performed with 120 projections/detector and 2 seconds/projection. By this means for the diagnostic scan there is preferential sampling of photons emanating from the heart, whereby a greater proportion of imaging time is allocated to collecting data from the heart at the expense of collecting fewer data from less important surrounding and remote regions. Conceptually this design is equivalent to allowing pixels of a conventional parallel collimator to acquire scintigraphic emissions from the heart for a longer time than pixels acquiring data from background structures.

Although due to its unique L-shaped geometry, the D-SPECT® camera can be positioned very close to the

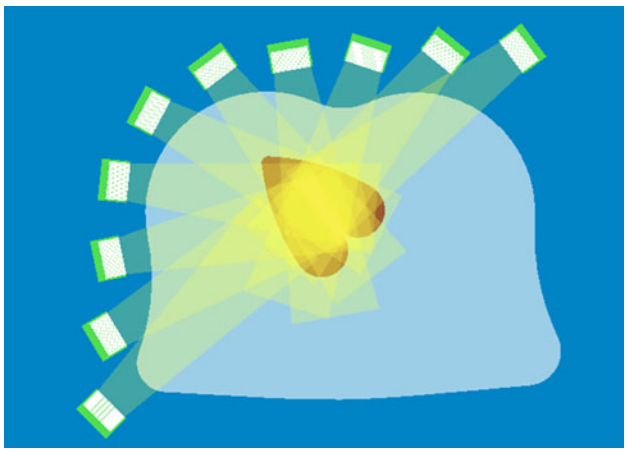

Figure 10. Schematic of the multiple scanning parallel-hole collimators of the D-SPECT® camera, focused on the region of the heart following a pre-scan to determine the heart's location. Courtesy, Spectrum Dynamics.

patient's chest wall, clearly the wide, short, square-hole collimator design described above would result in much poorer spatial resolution than that obtained using a conventional SPECT camera equipped with a high-resolution parallel-hole collimator. The loss of spatial resolution is compensated for by the use of a proprietary Broadview® software reconstruction algorithm based upon OSEM reconstruction, accurately modeling the probability function, supported by an increased number of viewing angles. Also, the reconstructed volume is fitted to a smooth ellipsoid-like surface, after which further iterations are performed, giving the myocardial walls a very thin appearance in typical D-SPECT® tomograms.[32]

Multi-pinhole collimation. The General Electric Discovery NM 530c® camera employees 19 8 × 8 cm detectors focused on the heart to sample photons emanating from the heart and the regions immediately around it (Figure 11). Each detector contains 32 × 32 pixilated 5-mm thick CZT elements. The detector assembly is mounted on a gantry that allows for patient positioning in either the supine or the prone position. The size of the CZT modules allows the camera to be positioned closely enough to the chest wall to ensure that the detectors provide 3-D sampling of the heart sufficient for tomographic reconstruction. The target volume is approximately a sphere of 19-cm diameter. The patient is positioned so that the heart is centered within this field-of-view. Each of the 19 detectors is composed of 4 solid-state CZT pixilated detectors mounted by a single tungsten pinhole collimator with a 5.1 mm effective diameter aperture.[33] Nine of the pinhole detectors are oriented perpendicular to the patient's long axis. Five are angled above, and five are angled below the axis, providing a 3-dimensional acquisition geometry. Each of the pinhole collimators simultaneously obtains an image of the heart, with no moving parts during data acquisition. Because the distance between the CZT detector and the pinhole is less than the distance between the pinhole and the heart, the cardiac image is minimized to preserve resolution, rather than maximized and distorted, as in the case of other nuclear medicine pinhole applications such as pinhole imaging of the thyroid or the hips.

Because the detectors and the patient are both stationary, there are no ''rotating'' planar projection images available to the interpreting physician to assess patient motion. Therefore, the location of the left breast and left hemidiaphragm as potential attenuators, and the location and intensity of subdiaphragmatic tracer concentration as a potential cause of Compton scatter into the inferior myocardial wall cannot be ascertained. However, a ''scan QC'' screen is provided that includes all pinhole views to aid the interpreting physician estimate the location of these attenuators. With multipinhole collimation the focal point of the collimators is within the thorax, so breast attenuation is less problematical than with parallel-hole collimation. However, the problems of diaphragmatic attenuation and subdiaphragmatic Compton scatter are not avoided. Since high counting statistics allow for dramatically reduced SPECT acquisition times (see below), several laboratories using the Discovery 530c® camera perform both supine and prone SPECT routinely on all patients to better assess inferior myocardial tracer distribution.

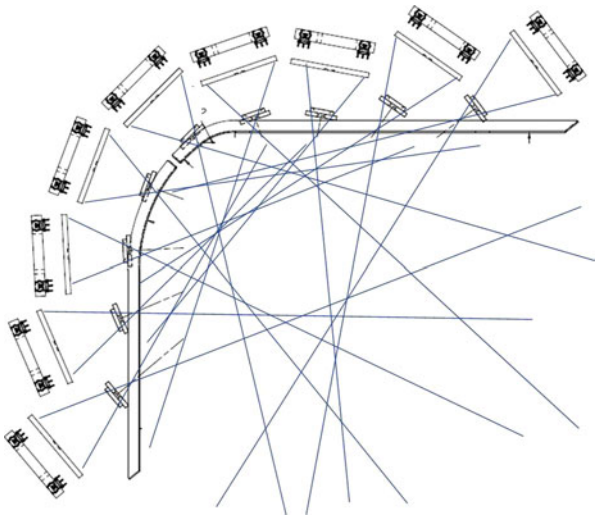

Figure 11. Schematic of the multiple focused pinhole collimator design of the Discovery NM 530c® camera, focused on the region of the heart. Spatial resolution is optimal at the focal depth of the collimators. Courtesy, General Electric Medical Systems.

Solid-State Detectors

Conventional sodium iodide scintillation cameras employ an array of photomultiplier tubes mounted behind the scintillation crystal. Typically photomultiplier tubes are hexagonal or square and measure approximately 46 cm^2. In general, there are over 50 photomultiplier tubes in modern scintillation cameras. When a photon strikes the sodium iodide crystal, a flash of light is emitted, which is detected by all the photomultiplier tubes. Those tubes closest to the scintillation event receive more light than more distant tubes. Each photomultiplier tube is a photocathode, which emits electrons when impacted by light. By means of a cascading dynode array, the number of electrons is then multiplied, producing an electrical current output at the back end of the photomultiplier tube. Those photomultiplier tubes closest to the scintillation event therefore produce a stronger electrical signal than the more distant tubes. The location of the scintillation event is then determined by electrical

positioning circuitry, which combines the analog output signals of all the photomultiplier tubes and computes a weighted average of all the signals as a function of position. This probabilistic method results in a Gaussian spatial distribution, estimating the location of the scintillation event.

As a result of this probabilistic approach, there is considerable uncertainty in localization of the scintillation event, resulting in blurring of the scintigraphic image and suboptimal spatial resolution. Also, the positioning circuitry is relatively slow, limiting the count-rate capabilities of conventional scintillation cameras. To compound this shortcoming, the efficiency of the photocathode of the photomultiplier tube in converting optical photons to electrons only about 20%. These combined factors result in relatively poor spatial resolution and sensitivity of conventional scintillation cameras.

In contrast, solid-state detectors are quantized, whereby the detector head is divided into an array of individual detector elements. Crosstalk between these pixilated detectors is minimal; therefore, when a scintigraphic event occurs each of the pixilated detectors produces an ''all or none'' output signal. The output is quantized and discrete rather than Gaussian, as in the case of conventional sodium iodide cameras. Therefore, the size and the spacing of the solid-state detector elements define the spatial resolution of the detector (Figure 12).

Indirect solid-state detectors. When gamma rays are converted to electrical charge indirectly, first with the gamma ray undergoing a scintillation event and being converted to light, then with the light converted to electron hole pairs, the conversion process is termed ''indirect.'' Indirect solid-state detectors are used in a wide variety of medical imaging applications including CT scanners and PET cameras. The only scintillation specifically camera designed for nuclear cardiology that employs indirect solid-state technology is the Digirad camera. The scintillator is cesium iodide (CsI), which has a good stopping power for low-energy gamma rays and emits more optical photons than sodium iodide. Scintillation events are detected using a pixilated detector array.[27] Each individual detector element (pixel) measures 6 mm × 6 mm × 6 mm. These detectors are arranged in 24 modules, each containing two 4 × 4 arrays. Thus, each camera head is composed of an array of 768 6-mm detector elements. Each CsI detector element is interfaced to a wafer-thin (0.3 mm) silicon photodiode semiconductor detector. The silicon photodiode has a high efficiency in converting optical photons to electrons. A bias voltage is applied across the semiconductor detector, resulting in electrical output when the photodiode is impacted by optical photons created by a scintillation event.

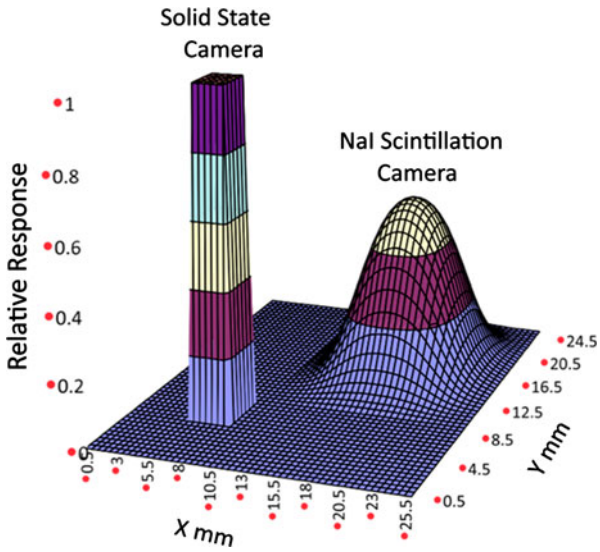

Figure 12. Schematic of the differences in spatial resolution provided by a solid-state detector as compared to a conventional NaI detector. With solid-state detectors the output is ''all or none,'' with resulting optimal spatial resolution. In contrast, using probabilistic positioning circuitry to process signals from an array of photomultiplier tubes, spatial resolution is poorer for NaI detectors, with blurring of object edges. Courtesy, Richard Conwell, Digirad Inc.

Direct solid-state detectors. In contrast to indirect semiconductor detectors, CZT provides ''direct'' solid-state technology. The CZT semiconductor is a pixilated array approximately 5-mm thick with an effective Z of 50 and a density of 5.8 g/cm^3. Gamma rays enter the CZT semiconductor detector and are directly converted to electron hole pairs. These charges (electrons and holes) then drift towards positive and negative electrodes, respectively, producing electrical output signals. Because not all the holes and the electrons drift towards the negative and the positive electrodes at the same rate, some of the holes get delayed or ''trapped'' in the semiconductor material. This results in incomplete charge collection, in turn resulting in a broadening of the photopeak on the low-energy side. This ''hole-tailing'' effect varies from pixel to pixel within the array, but in general becomes more marked with increasing thicknesses of semiconductor material. For that reason, although CZT is more dense than sodium iodide (5.8 vs 3.7 gm/cm^3), the thickness of the CZT detector must be kept to a minimum ($\sim$5 mm). In this configuration, the CZT detector has excellent energy resolution (FWHM = 5.4%, compared to a FWHM = 9.4% for a conventional sodium iodide camera). With such improved energy resolution it is possible to clearly separate photons of Tc-99m (140 keV) and iodine-123 (160 keV) (Figure 13). Similarly, the composite 70 keV photopeak and 81 keV lines of thallium-

201 are clearly resolved.[34] However, due to the necessary thinness of the CZT detector, its intrinsic efficiency for detecting 140 keV gamma rays is only approximately equivalent to that of a conventional sodium iodide detector (88% vs 90%). Additionally, to overcome the effects of the variation of hole-tailing per pixel, energy windows in CZT cameras are often set relatively wide, as in conventional sodium iodide cameras, to ±10%, making their scatter fraction performance similar to conventional sodium iodide cameras.[35]

Attenuation Correction

AC for myocardial perfusion SPECT has been available for over a decade, and therefore cannot truly be considered a ''new advancement.'' However, technical advancements in AC now allow for reduced patient radiation dose associated with x-ray emission scans. Diagnostic quality CT imaging of the chest is not necessary for AC. An attenuation map adequate for AC can be generated using a lower mA and kVp. By this means state-of-the-art technology for AC of myocardial perfusion SPECT affords the patient only approximately 0.2-0.4 mSv.

A novel, ultra-low-dose AC method has been incorporated into the Digirad Cardius X-ACT® camera.[27] After the emission scan has been acquired, the camera's three detectors are automatically reconfigured to form a single large 27-inch transaxial detector arc. The focal line of the collimator of each head co-aligns

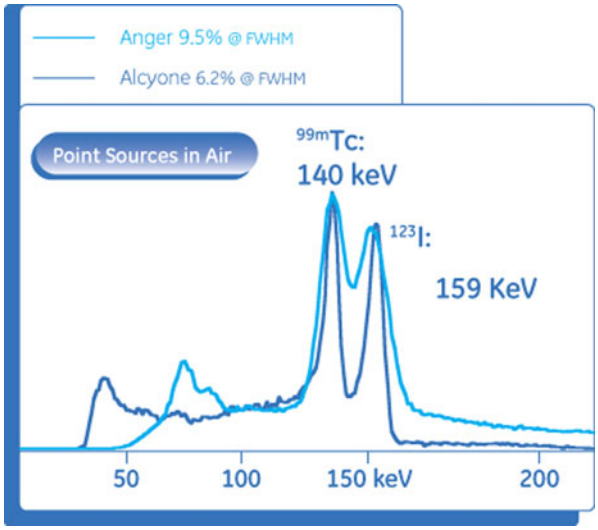

Figure 13. Pulse height spectra for Tc-99m and I-123 obtained using a conventional NaI Anger camera and a CZT solid-state detector (Alcyone, Discovery NM 530c® camera). The two isotope peaks are discriminated much more effectively using the CZT detector. Courtesy, General Electric Medical Systems.

with the spatial location of a fluorescent x-ray transmission line source to form a fan-beam transmission acquisition geometry. During the transmission scan the chair on which the patient sits first rotates 206° for 60 seconds with the transmission source on in order to acquire the transmission data, then rotates 206° for 60 seconds in the reverse direction with the transmission source off to acquire the contamination data from emission sources in the patient to the transmission data. The resulting attenuation map is of poor spatial resolution (relative to a diagnostic CT machine), but adequate to correct the Tc-99m cardiac emission scan for soft tissue and blood pool attenuation. The associated patient radiation dose is only approximately 5 μSv. A limitation of this method, shared by all other x-ray attenuation techniques, is that the emission and subsequent transmission scans are sequential, allowing the possibility of patient motion between the emission and the transmission scans and misregistration of the two. Due to the longer acquisition time for the low-flux fluorescent x-ray transmission scan, the opportunity for patient motion is somewhat greater. Fortunately, however, software is available to easily register the emission and the transmission scans.

It should be emphasized that the increased count-rate statistics and improved image quality obtained with the new hardware methods described above are a result of combined advancements in both hardware and software. Spatial resolution for SPECT imaging of Tc-99m has been evaluated for the three new cameras described above, all of which combine hardware and software innovations. For the Digirad Cardius® detector head the extrinsic planar resolution (FWHM) at 10 cm with scatter was determined to be 9.9 mm with a LEHR collimator and 10.6 mm with a LEAP collimator. Defect contrast of the Data Spectrum phantom full defect was 0.528.[27] For the Spectrum Dynamics D-SPECT® camera, for a single line source the FWHM was demonstrated to be 3.5 mm in the *x*-axis and 4.2 mm in the *y*-axis, as compared to 9.2 and 12.5 mm, respectively, for conventional SPECT.[32] Compared to a standard SPECT system, the D-SPECT camera was demonstrated to have energy resolution ~2 times better, a point-source sensitivity ~5 times higher, and a superior count-rate capability.[36] For the General Electric Discovery NM 530c® camera SPECT resolution at 15 cm evaluated using three point sources with scatter was determined to be 5.4 mm, compared to 9.4 mm for conventional SPECT with a dual-head state-of-the-art NaI detector.[37] It should be emphasized that since these experiments evaluating system performance were performed independently for each of the cameras, not necessarily with settings used for clinical imaging, and since experimental parameters differed for each system,

it is not possible to draw direct comparisons. In fact, efforts to perform a more representative comparisons show that the performance of these cameras are very similar.[38,39] Nevertheless, these innovative cameras, which combine advancements in detector characteristics, collimation, and SPECT processing software, represent a tremendous advancement in the field of Nuclear Cardiology, enabling a significant decrease in image acquisition time, radiopharmaceutical dose, or both.

CLINICAL RESULTS

Software Methods

In a single-center study of 50 patients, Borges-Neto et al[15] reported similar myocardial perfusion SPECT quality using WBR® (UltraSPECT, Ltd.) ''half-time'' software compared to standard ''full-time'' SPECT acquisitions acquired on a standard dual-head sodium iodide detector and processed with FBP. Subsequently, in a prospective series of 156 patients DePuey et al[16] reported that the image quality of gated perfusion SPECT obtained with both Evolution® software (General Electric Medical Systems), incorporating OSEM and resolution recovery, and ''half-time'' WBR® software, incorporating these advancements as well as noise compensation, were both equivalent or superior to gated full-time FBP scans (Figures 14, 15). However, these authors observed that left ventricular functional parameters determined by both of these ''half-time'' methods differed significantly from those derived from ''full-time'' FBP processing. LVEF's averaged 3-9 points lower with ''half-time'' processing compared to those obtained using ''full-time'' FBP processing. Basso et al[40] reported similar results in a series of 47 patients. Reduced-time WBR® yielded image quality superior to that obtained with full-time FBP. In patients with perfusion defects summed difference scores (SDSs) were similar by both methods, but as reported by DePuey et al, LVEFs were 9%-10% lower with the WBR® method. In a prospective trial, Marcassa et al[41] studied 52 patients undergoing a rest/stress Tc-99m sestamibi protocol with ''full-time'' SPECT processed with FBP and ''half-time'' SPECT processed with WBR®. In addition, 40 other patients received half the usual radiopharmaceutical dose and underwent ''double-time'' SPECT processed with FBP and ''full-time'' SPECT processed with WBR®. These investigators reported that for either the ''full-dose/half-time'' or

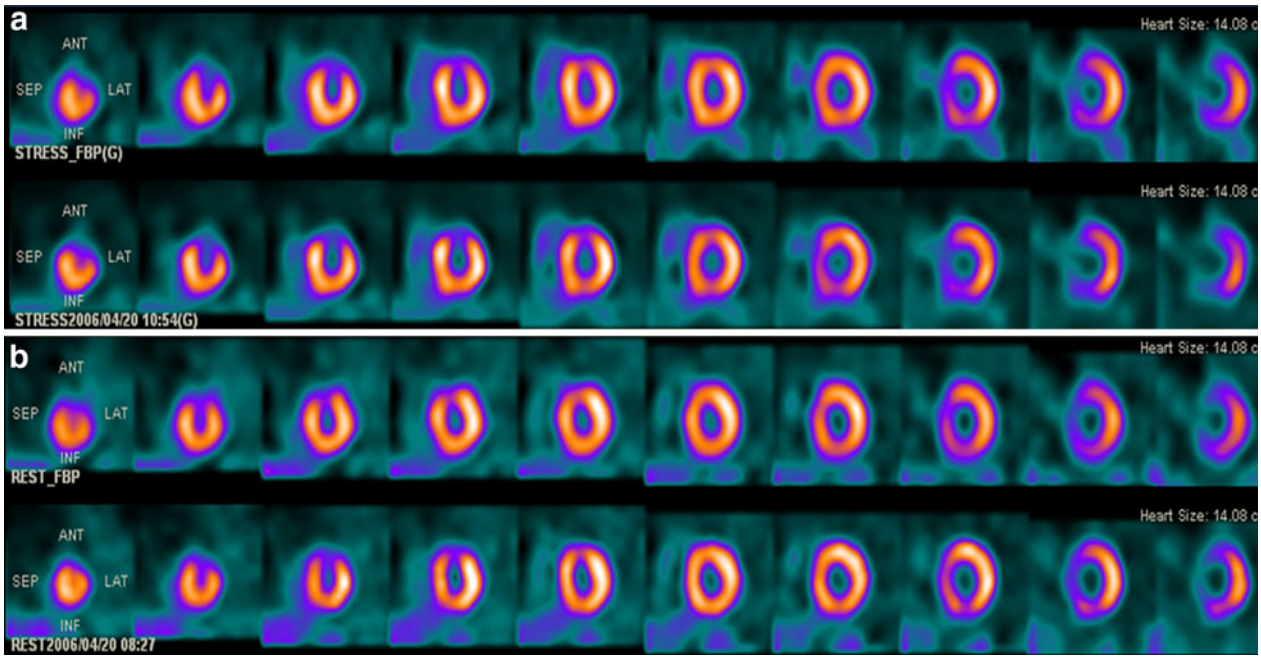

Figure 14. Comparison of myocardial perfusion stress (**A**) and rest (**B**) SPECT acquired ''full-time'' and processed with FBP (*top row*), compared to ''half-time'' SPECT processed with Evolution® software (*bottom row*), incorporating OSEM iterative reconstruction and resolution recovery. A single-day rest/stress 9/32 mCi Tc-99m sestamibi protocol was used. Image quality and resolution of the fixed anterior perfusion defect in this patient with a documented prior myocardial infarction is equivalent using the ''full-time'' and ''half-time'' acquisition and processing techniques. Courtesy Gordon DePuey, St. Luke's-Roosevelt Hospital, New York, NY.

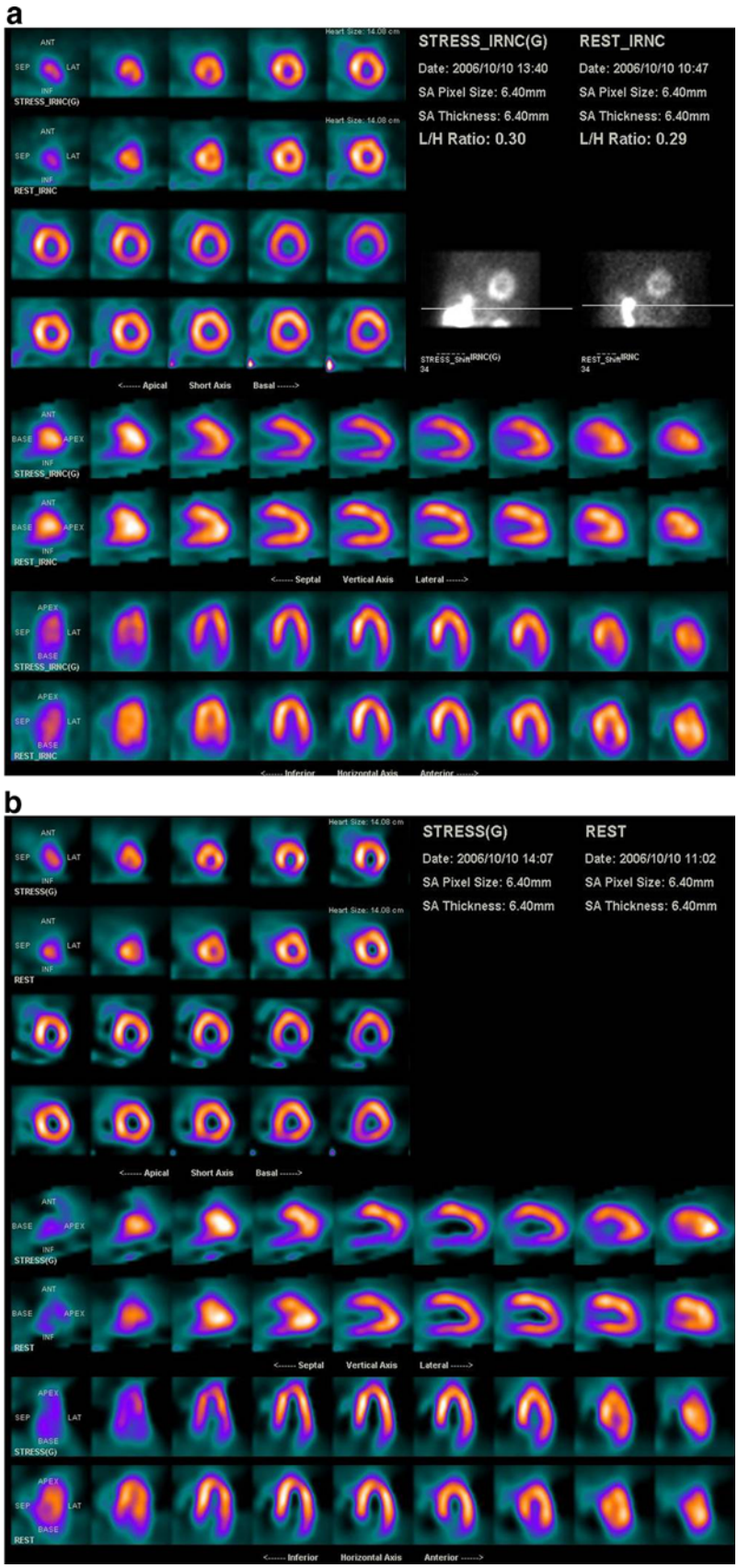
a
STRESS_IRNC(G)
Date: 2006/10/10 13:40
SA Pixel Size: 6.40mm
SA Thickness: 6.40mm
L/H Ratio: 0.30
REST_IRNC
Date: 2006/10/10 10:47
SA Pixel Size: 6.40mm
SA Thickness: 6.40mm
L/H Ratio: 0.29
<------ Apical Short Axis Basal ------>
<------ Septal Vertical Axis Lateral ------>
<------ Inferior Horizontal Axis Anterior ------>
b
STRESS(G)
Date: 2006/10/10 14:07
SA Pixel Size: 6.40mm
SA Thickness: 6.40mm
REST
Date: 2006/10/10 11:02
SA Pixel Size: 6.40mm
SA Thickness: 6.40mm
<------ Apical Short Axis Basal ------>
<------ Septal Vertical Axis Lateral ------>
<------ Inferior Horizontal Axis Anterior ------>

◀**Figure 15.** Comparison of myocardial perfusion stress SPECT acquired ''full-time'' and processed with FBP (**A**), compared to ''half-time'' SPECT processed with WBR® software, incorporating OSEM iterative reconstruction, resolution recovery, and noise compensation (**B**). A single-day rest/stress 9/32 mCi Tc-99m sestamibi protocol was used. Image quality and resolution of the reversible inferior perfusion defect in this patient with a documented RCA stenosis is superior using the ''half-time'' acquisition and processing techniques. Comparing gated post-stress SPECT image quality for the ''full-time'' (**C**) and ''half-time'' (**D**) techniques, the former provided better image quality with superior definition of the endocardial borders. Courtesy Gordon DePuey, St. Luke's-Roosevelt Hospital, New York, NY.

''half-dose/full-time'' WBR® methods image quality and defect characteristics (SSSs) did not differ significantly from standard acquisition and FBP processing methods.

In a prospective study reported by Druz et al,[42] 434 patients underwent ''full-time'' (20 second/stop) dual-isotope Tl-201/Tc-99m sestamibi SPECT processed with FBP, followed by half-time (10 second/stop) SPECT processed with WBR®. For experienced nuclear cardiologist interpreting the scans diagnostic certainty was better for the ''half-time'' WBR® scans. The percentage of ''equivocal'' interpretations decreased from 35 to 9 ($P < .0001$). In a subgroup of patients who underwent coronary angiography, there were no differences in diagnostic sensitivity, specificity, or accuracy between the two methods.

Using Astonish® software developed by Phillips, incorporating resolution recovery and a different reduced-time software processing method, in a series of 221 patients in whom ''half-time'' acquisitions were simulated by dropping every other frame/stop of data during a 180° SPECT acquisition, Venero et al observed myocardial perfusion defect characteristics to be nearly identical to the ''full-time'' and simulated ''half-time'' techniques. Left ventricular functional parameters correlated well using the standard and reduced-time methods[43] (Figure 16). ''Half-time'' SPECT simulated with this ''data stripping'' method combined with Gd-153 line-source AC has also been reported to improve diagnostic certainty as compared to non-attenuation-corrected simulated ''half-time'' SPECT.[44]

In a later report, DePuey et al[45] imaged 209 patients prospectively at rest and following exercise or pharmacologic stress (9/32 mCi ^{99m}Tc-sestamibi) full-time processed with OSEM, and again ''quarter-time'' processed with a modified WBR® algorithm (Xpress-3®, UltraSPECT, Ltd.), incorporating a noise compensation technique more rigorous than the one employed for the previously described ''half-time'' technique (Figure 17). Blinded observers graded scan quality (1 = poor to 5 = excellent) based on myocardial uniformity, endocardial/epicardial edge definition, and background noise. Perfusion defects were scored using a 17-segment model. Using three commercially available software methods, EDV, ESV, and LVEF were calculated. They demonstrated that by employing this more rigorous noise compensation algorithm ''quarter-time'' perfusion SPECT afforded image quality, defect characterization, and functional assessment equivalent to full-time OSEM, providing the potential for even more markedly decreased SPECT acquisition times and/or radiopharmaceutical doses. However, just as described above for WBR® ''half-time'' processing, these authors observed that left ventricular functional parameters determined by ''quarter-time'' WBR® averaged 3-9 points lower than those obtained using ''full-time'' OSEM processing. They postulated that the lower LVEFs obtained with ''quarter-time'' WBR® resulted from more accurate tracking of the motion of the left ventricular valve plane during ventricular systole, and therefore seemed to better correspond to visual estimation of LVEF. Consequently, they recommended that when following an individual patient, the same acquisition and processing methods should be used to determine functional parameters. Ideally, normal databases should be determined for each commercially available method used to determine left ventricular functional parameters.

Subsequently, using ''half-time'' WBR® software, DePuey et al[46] studied 156 consecutive patients in whom rest and 8-frame gated post-stress myocardial perfusion SPECT were performed following 9-12 mCi and 32-40 mCi Tc-99m sestamibi injections, respectively, with full-time (rest = 14 minutes; stress = 12.3 minute) acquisitions processed with OSEM, and also separate ''half-time'' acquisitions processed with WBR®. A separate group of 160 consecutive patients matched in gender, weight, and chest circumference received ''half-dose'' rest and stress injections (5.8 ± 0.6 and 17.5 ± 2.5 mCi) with full-time SPECT acquisitions. Image quality was again scored based upon myocardial count density and uniformity, endocardial edge definition, perfusion defect delineation, right ventricular visualization, and background noise. ''Half-time'' and ''half-dose'' WBR® non-gated and gated image quality were both superior to standard full-time OSEM (P's $< .001$). Mean image quality for rest, stress, and post-stress gated images were similarly excellent for ''half-time'' and ''half-dose'' WBR® (Figure 18). There was no significant difference between the summed stress and the rest scores for ''full-time'' OSEM versus ''half-time'' WBR® in 82 patients with perfusion defects. Therefore, these authors concluded that software methods that cope with reduced myocardial perfusion SPECT count density can be applied

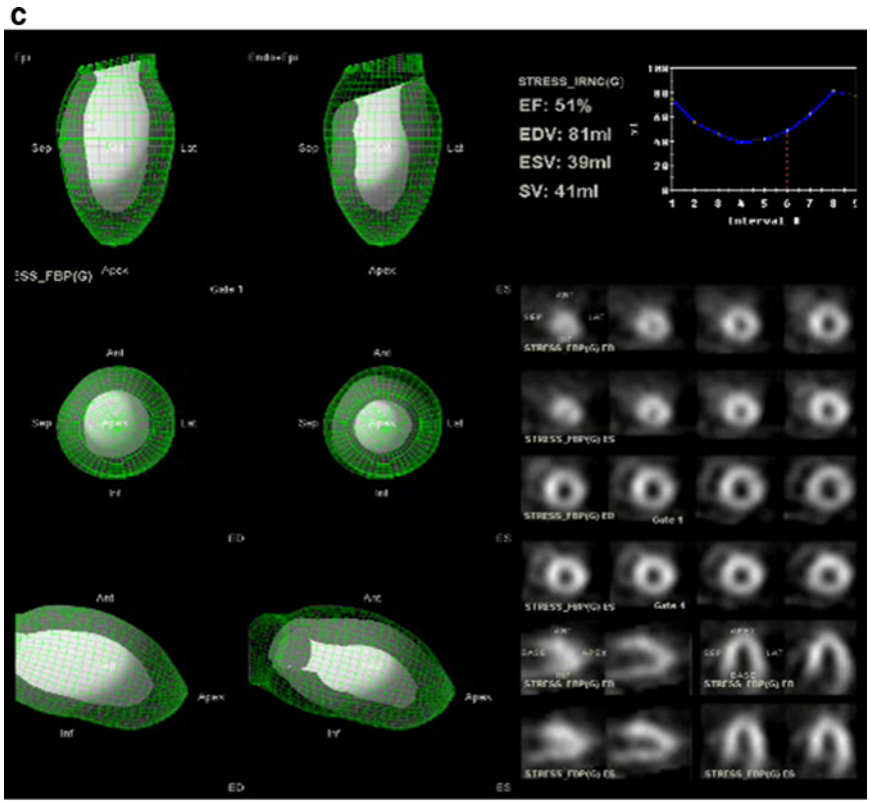

Figure 15. continued.

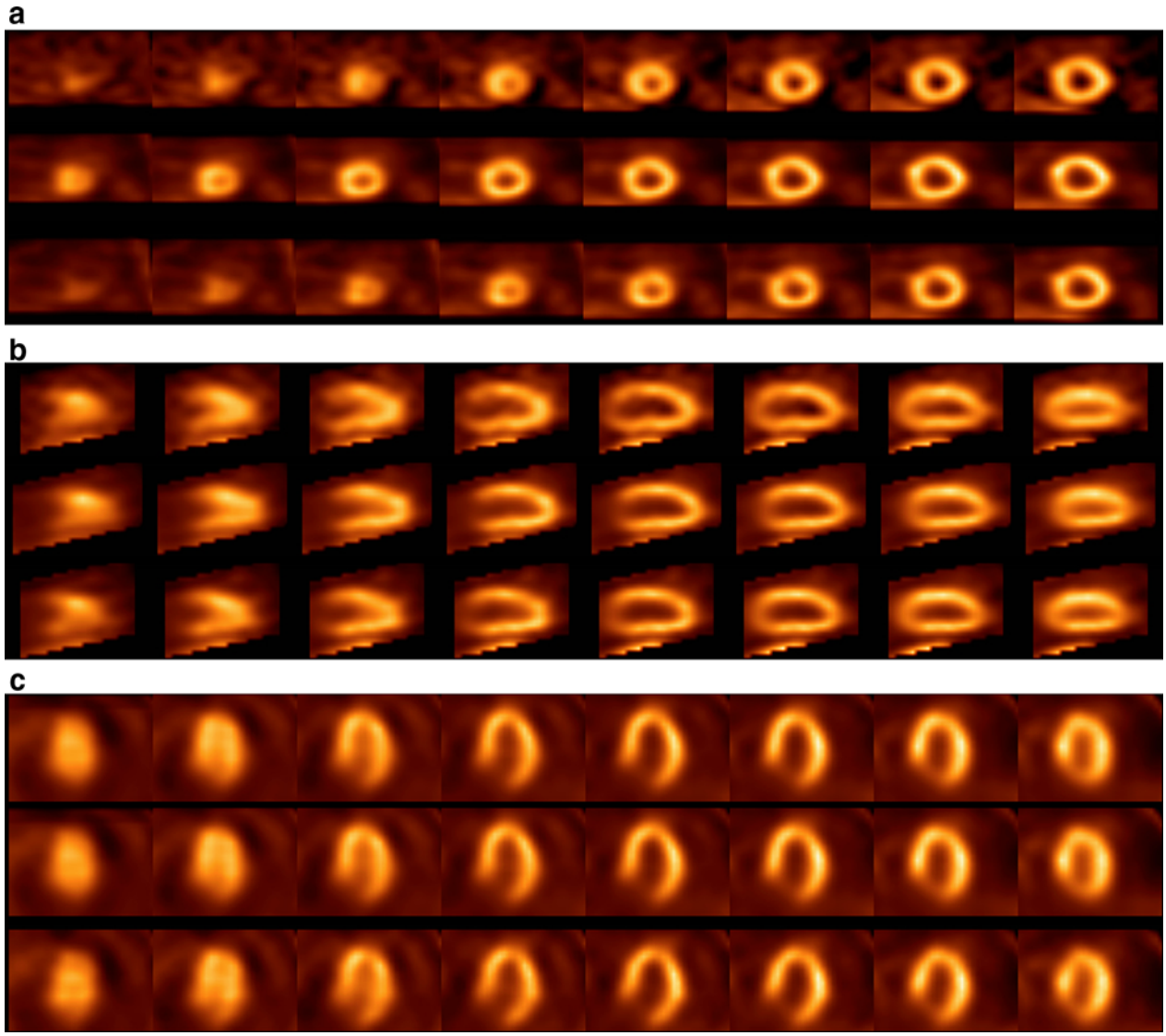

Figure 16. Comparison of myocardial perfusion stress SPECT from a normal subject acquired ''full-time'' and processed with FBP (*top row*), and with reduced count density Astonish® software, incorporating OSEM iterative reconstruction and resolution recovery (*middle row*). By means of ''data stripping'' a ''half-time'' SPECT acquisition was simulated, which was also processed with Astonish® software (*bottom row*). Short axis (**A**), vertical long axis (**B**), and horizontal long axis (**C**) tomograms are displayed. Image quality and resolution are equivalent for the ''full-time'' and ''half-time'' techniques.[42] Courtesy Gary Heller, Hartford Hospital, Hartford, CT.

equally well to reduced-time or reduced radiopharmaceutical dose scans.

Combined Hardware and Software Methods

Using the IQ SPECT® cardio-focused collimator in conjunction with Flash-3D® reduced count density reconstruction software (Siemens Medical Solution) and AC, Vija et al[28,29] demonstrated in Data Spectrum phantoms studies and one clinical patient example that myocardial perfusion SPECT image quality was comparable in 4-minute IQ SPECT® scans as compared to standard 20-minute acquisitions acquired with a LEHR collimator (Figure 19).

In a prospective, multi-center trial of 448 patients in whom full-time gated SPECT acquisitions and simulated ''half-time'' acquisitions were compared qualitatively and quantitatively with regards to perfusion defect characteristics and functional parameters, Maddahi et al[47] reported the results of reduced-time myocardial perfusion SPECT acquired on the Cardius® upright

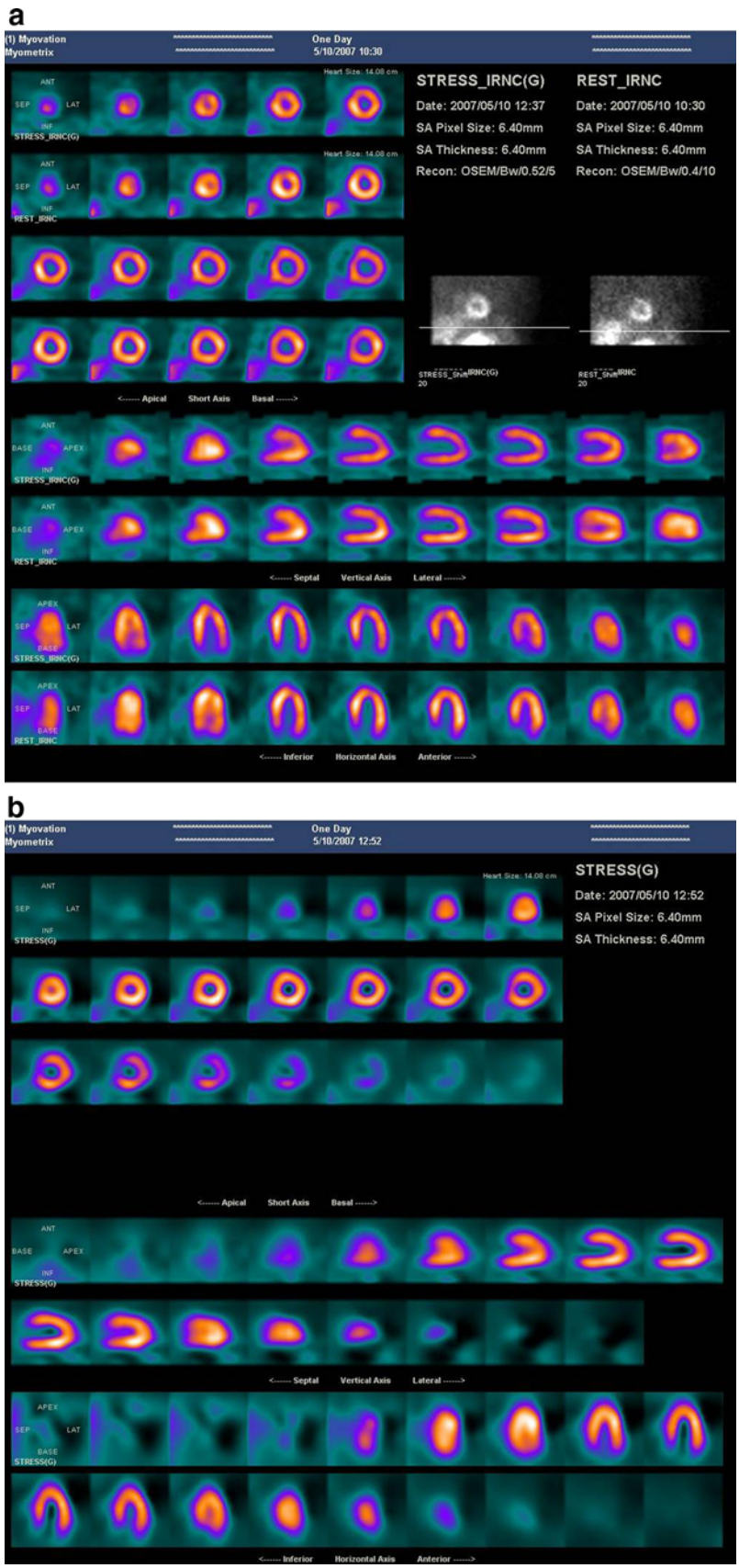
a
(1) Myovation
Myometrix
One Day
5/10/2007 10:30
STRESS_IRNC(G)
Date: 2007/05/10 12:37
SA Pixel Size: 6.40mm
SA Thickness: 6.40mm
Recon: OSEM/Bw/0.52/5
REST_IRNC
Date: 2007/05/10 10:30
SA Pixel Size: 6.40mm
SA Thickness: 6.40mm
Recon: OSEM/Bw/0.4/10
<------ Apical Short Axis Basal ------>
<------ Septal Vertical Axis Lateral ------>
<------ Inferior Horizontal Axis Anterior ------>
b
(1) Myovation
Myometrix
One Day
5/10/2007 12:52
STRESS(G)
Date: 2007/05/10 12:52
SA Pixel Size: 6.40mm
SA Thickness: 6.40mm
<------ Apical Short Axis Basal ------>
<------ Septal Vertical Axis Lateral ------>
<------ Inferior Horizontal Axis Anterior ------>

◀**Figure 17.** Comparison of myocardial perfusion stress and rest SPECT in a normal patient acquired ''full-time'' and processed with OSEM iterative reconstruction (**A**), compared to ''quarter-time'' stress SPECT processed with WBR® X-press 3® software, incorporating OSEM iterative reconstruction, resolution recovery, and a more rigorous noise compensation (**B**). A single-day rest/stress 9/32 mCi Tc-99m sestamibi protocol was used. Image quality and resolution are superior using the ''quarter-time'' acquisition and processing techniques. Comparing gated post-stress SPECT image quality for the ''full-time'' OSEM (**C**) and ''half-time'' WBR® (**D**) techniques, the former provided better image quality with superior definition of the endocardial borders. Courtesy Gordon DePuey, St. Luke's-Roosevelt Hospital, New York, NY.

camera employing CsI solid-state detectors and reduced count density nSPEED® software, incorporating OSEM reconstruction and resolution recovery (Digirad, Inc). They demonstrated that reduced-time acquisition image quality was at least as good as, and often superior to that obtained with full-time acquisitions. In 19.2% of stress tomograms and 19.4% of resting tomograms nSPEED® image quality was superior to standard SPECT image processing. The two techniques provided diagnostically equivalent images (Figure 20). Quantitative perfusion defect severity was not significantly different. These authors also observed an excellent correlation (r's $\geq$ 0.96) of functional parameters (LVEF, EDV, and ESV) comparing these two acquisition methods. The implication is that this new halftime method can be substituted reliably for full-time SPECT acquisition. Complementing the ability to preserve excellent image quality despite lower counting statistics, the Cardius X-ACT® upright camera incorporates advantages of upright, cardiocentric imaging, and low-dose AC (Figure 21).

The initial clinical validation of the D-SPECT® camera was reported by Sharir et al[48] in a single-center prospect of series of 44 patients who underwent a single-day stress/rest Tc-99m sestamibi protocol. Patients underwent conventional SPECT with 16- and 12-minute acquisitions and also high-speed D-SPECT® 4- and 2-minute acquisitions. Image quality of the D-SPECT® images acquired in much less time were excellent, and there was a close linear correlation between summed stress scores (SSSs) and summed rest scores (SRSs) (r's = 0.93, P's = .0001) determined by semiquantitative visual analysis (Figure 22). Diagnostic confidence in image interpretation was also similar for the two modalities.

This initial evaluation of the D-SPECT camera was followed by a large multi-center trial in which 238 patients underwent myocardial perfusion SPECT using a variety of exercise and pharmacologic stress single- and dual-isotope protocols.[49] A variety of commercially available standard scintillation cameras was used to acquire rest and stress SPECT acquisitions for approximately 20 and 15 minutes, respectively. D-SPECT® acquisitions were also acquired on all patients for 4 and 2 minutes, respectively. An additional 63 patients with a low pre-test likelihood of coronary artery disease were studied to establish method- and gender-specific normal limits. These investigators demonstrated an excellent correlation between quantitative total perfusion stress and rest defect scores for the two separate imaging modalities (r's = 0.95 and 0.97, respectively, P's < .0001) and excellent correlations for post-stress ejection fraction and end-diastolic volumes (r's = 0.89 and 0.97, respectively). There was also a good concordance with regards to assignment of perfusion abnormalities to specific vascular territories (>90% agreement). They concluded that the D-SPECT® high-speed technology provides quantitative measures of myocardial perfusion and function comparable to those with conventional SPECT in approximately 1/7th of the acquisition time.

The initial clinical validation of the Discovery NM 530c® solid-state camera was reported by Esteves et al.[33] One hundred sixty-eight patients underwent a single-day rest/stress Tc-99m tetrofosmin protocol. All patients were imaged using conventional dual-detector cameras for 14 minutes for gated resting imaging and 12 minutes for gated post-stress imaging. Similar gated SPECT imaging datasets were acquired on the Discovery® camera but with acquisition times of only 4 and 2 minutes, respectively (Figure 23). There was a >90% correlation in interpretation of the presence or the absence of perfusion defects on a per-patient basis. Correlation coefficients of rest and stress left ventricular ejection fractions were 0.87 and 0.90, respectively. Similarly, excellent correlations were reported for rest and stress end-systolic and end-diastolic volumes (r's $\geq$ 0.94). These and other investigators concluded that the Discovery NM 530c® solid-state camera allows a more than 5-fold reduction in scan time and provides clinical perfusion and function information equivalent to conventional dual-head SPECT.[50]

Taking advantage of the Discovery® camera's list-mode capabilities, Herzog et al[51] reconstructed SPECT scans of varying duration from 1 to 6 minutes and compared results visually and semiquantitatively to full-time SPECT scans acquired on a standard dual-head NaI detector camera to determine an optimal scan acquisition time. Their results revealed that optimal imaging times are 3 minutes for resting SPECT and 2 minutes for post-stress SPECT using a conventional single-day low-dose rest/high-dose stress protocol. In a large retrospective study, Duval et al compared the myocardial count density and overall quality of low-dose Tc-99m sestamibi stress-only myocardial perfusion

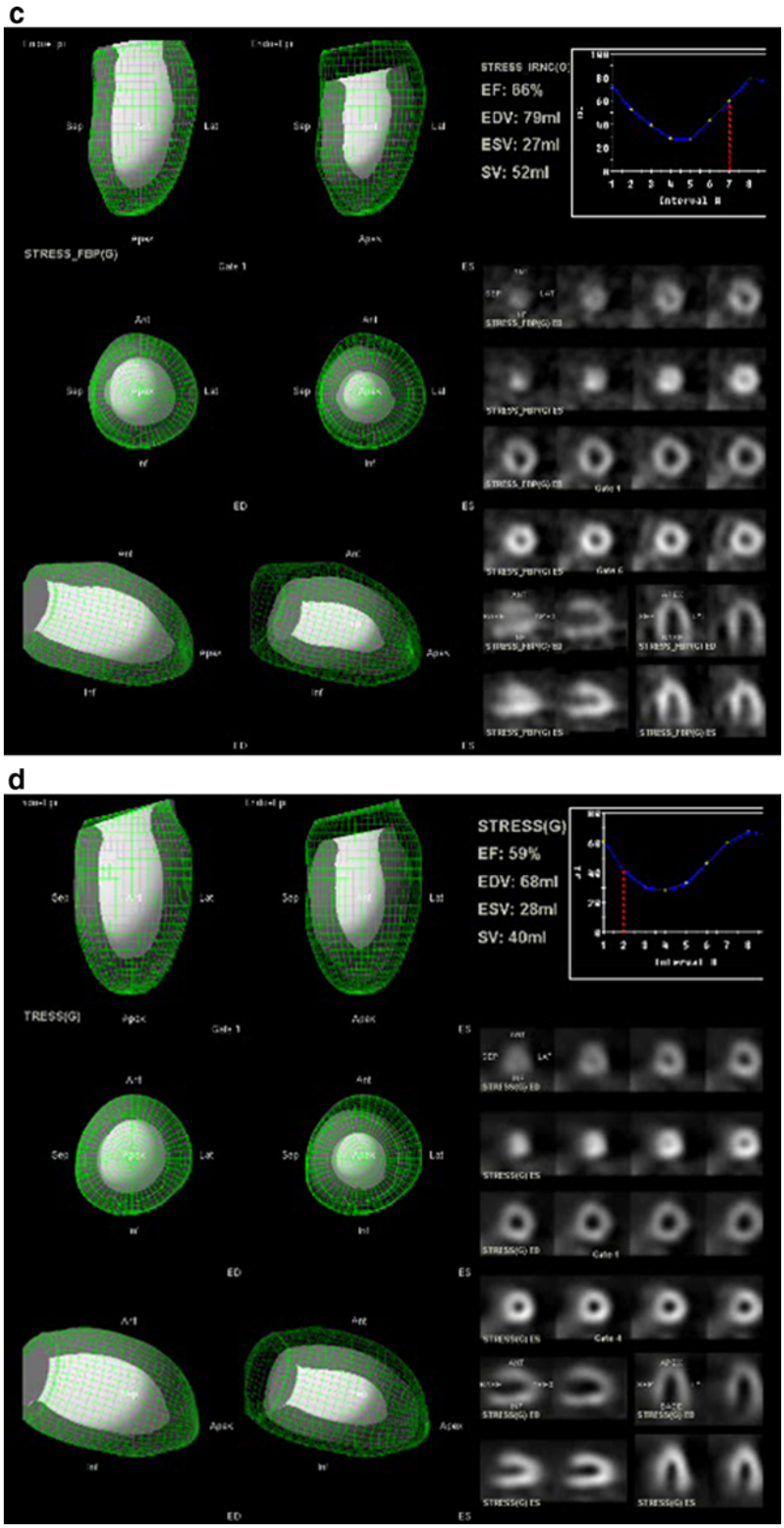

Figure 17. continued.

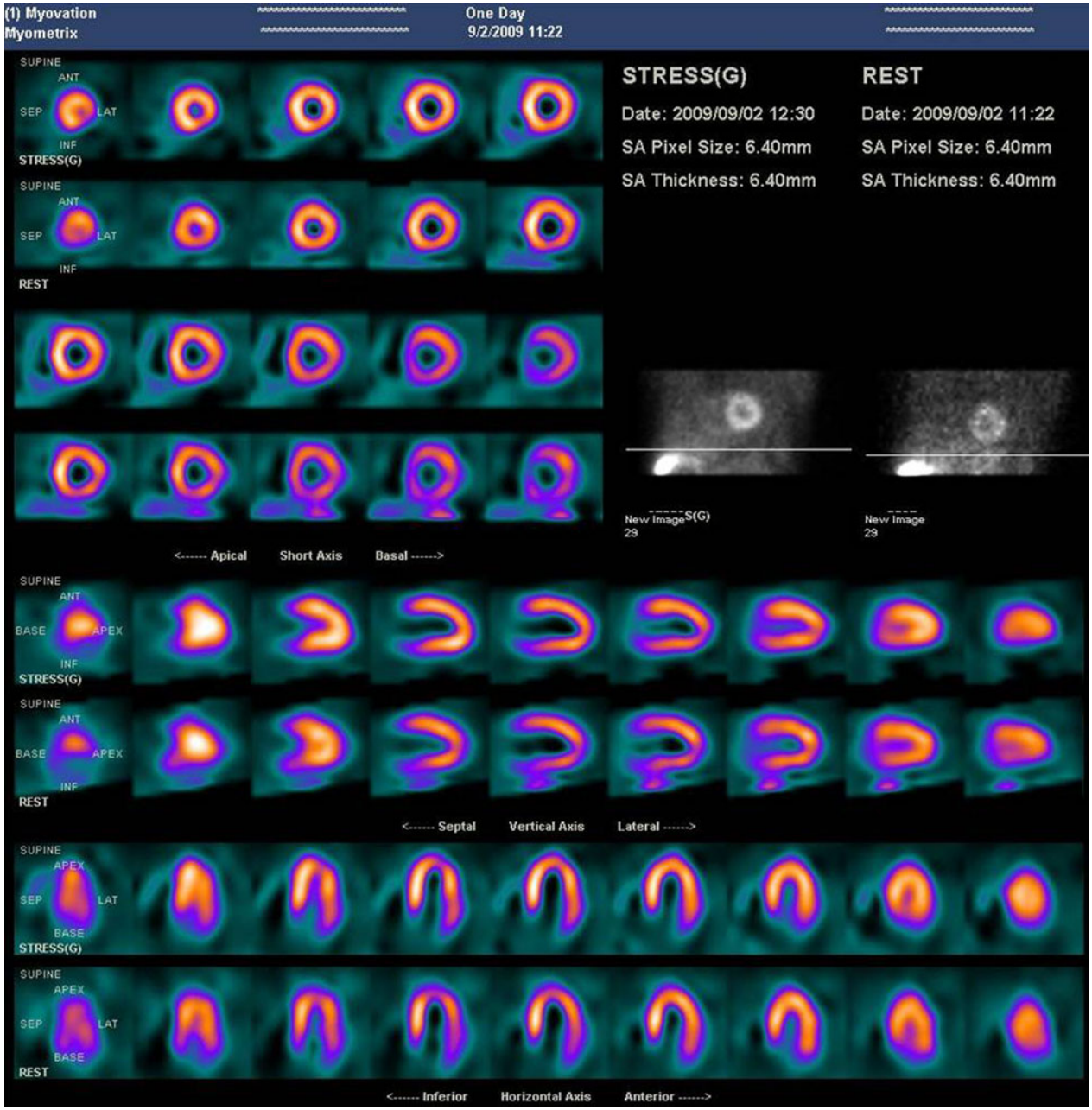

Figure 18. WBR® ''half-time'' Xpress® software was used to reconstruct this reduced-dose rest/stress (6.2/17.3 mCi) Tc-99m sestamibi ''full-time'' SPECT scan in a normal male patient with a 38″ chest circumference. Image quality is excellent and comparable to a ''full-dose,'' ''full-time'' study processed with OSEM iterative reconstruction[46].

SPECT (209 patients) with high-dose stress-only SPECT (140 patients) and with high-dose stress SPECT images acquired as part of a standard low-dose rest/high-dose stress protocol (368 patients).[52] The average injected Tc-99m sestamibi activities were 12.5, 29.2, and 41.7 mCi, respectively. SPECT imaging acquisition times were 3 minutes for the low-dose patients and 5 minutes for the other two patient groups. These authors observed that the myocardial count density and image quality of the low-dose 5-minute scans were equivalent to those in the other two groups in which the injected dose was higher and the image acquisition time was shorter. Moreover, as discussed below, using this protocol they documented the feasibility of performing a stress-only

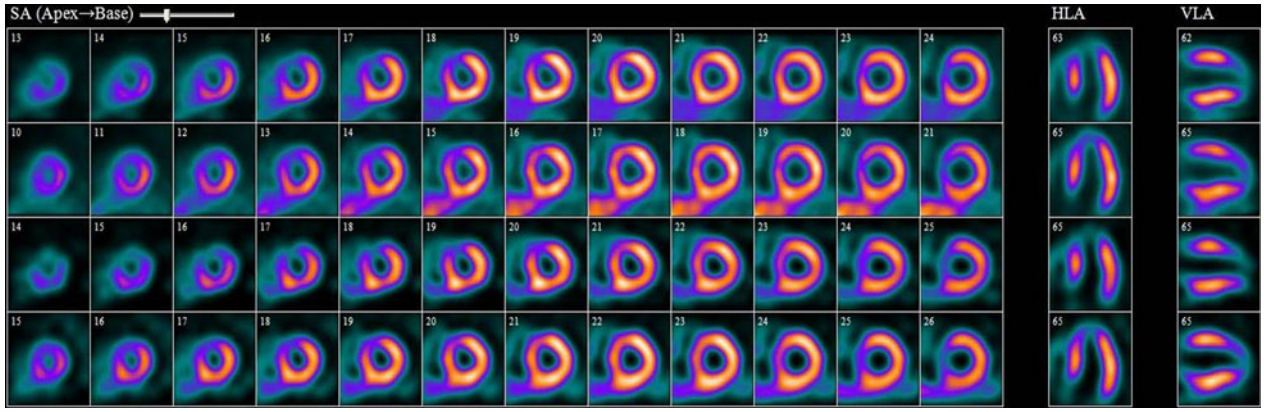

Figure 19. In this patient with an anterior/apical myocardial infarct SPECT was acquired first with a parallel-hole collimator with AC, and then with the IQ SPECT® collimator and AC. Stress and rest SPECT acquisition times were 15 and 20 minutes, respectively, for the parallel-hole collimator acquisitions; and 4 and 4 minutes, respectively, for the IQ SPECT® acquisitions. CT AC was performed with an exposure of 0.2-0.4 mSv. *Top row* parallel-hole stress with AC; *second row* parallel hole rest with AC; *third row* IQ SPECT® stress with AC; *fourth row* IQ SPECT® rest with AC. Courtesy James Corbett, University of Michigan, Ann Arbor, MI.

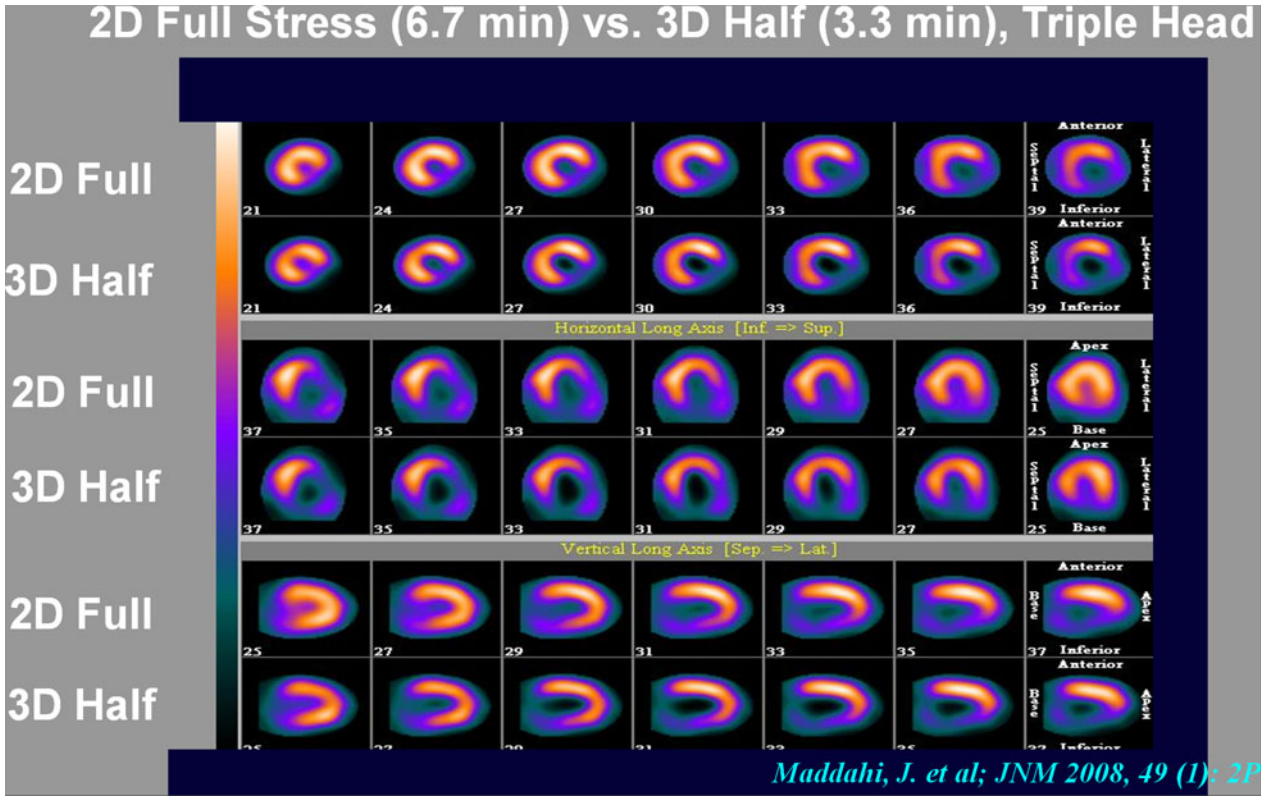

Figure 20. In this patient with an extensive inferolateral infarct SPECT was acquired on an upright Digirad solid-state detector camera. Images were acquired simultaneously ''full-time'' (*top row* of each orthogonal tomogram) and ''half-time'' (*bottom rows*). ''Full-time'' SPECT was processed with OSEM iterative reconstruction. ''Half-time'' SPECT was processed with nSPEED® software, incorporating resolution recovery and noise compensation. Image quality is slightly superior for the ''half-time'' technique. Courtesy Jamshid Maddahi, David Geffen School of Medicine at UCLA, Los Angeles, CA.

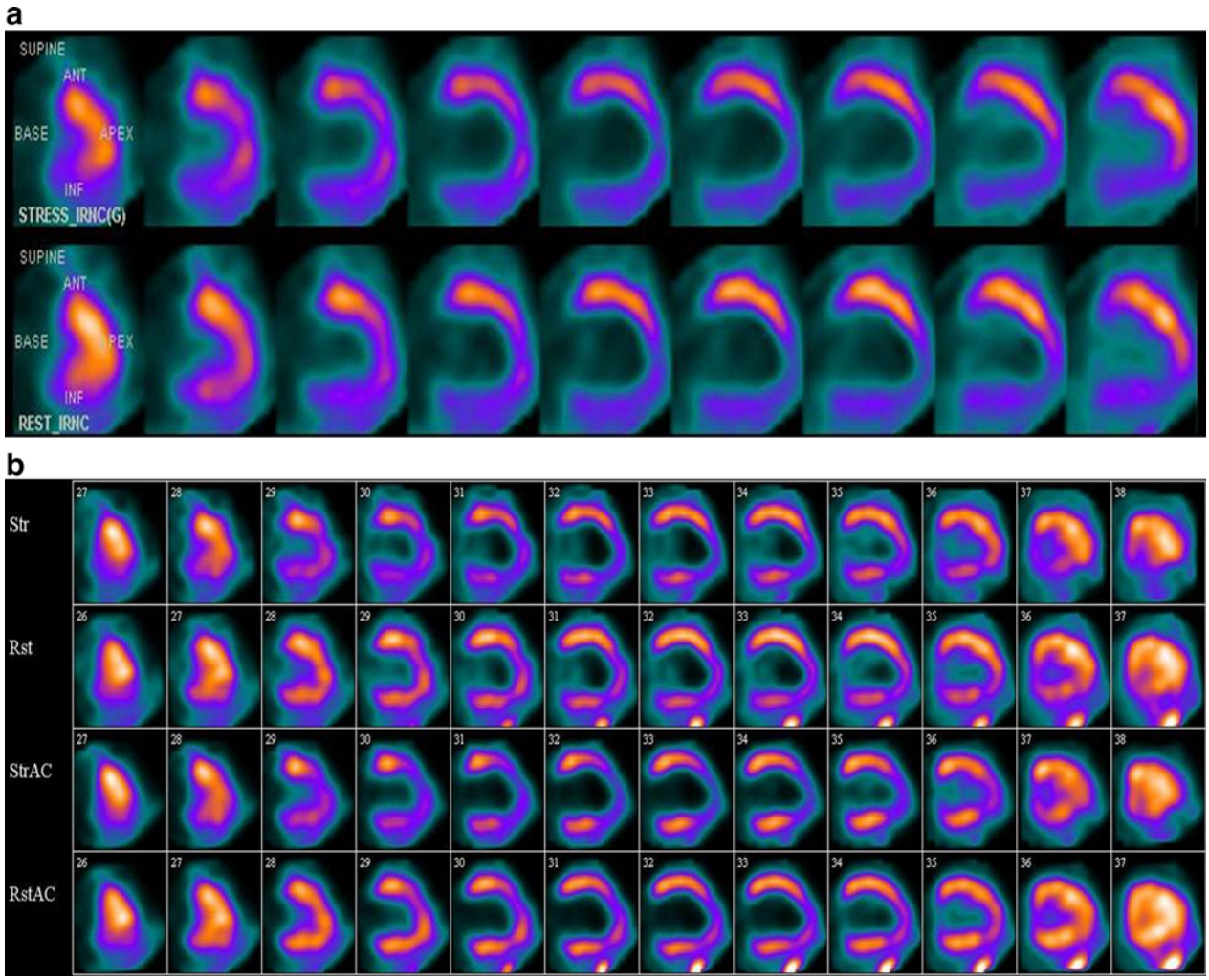

Figure 21. **A** Stress (*top row*) and rest (*bottom row*) supine SPECT was performed in this patient with an ischemic cardiomyopathy using a conventional dual-head NaI detector. In these vertical long axis tomograms the ventricle is markedly dilated, and there appear to be extensive, fixed perfusion abnormalities involving the apex and inferior wall. **B** The stress and rest (first and second rows, respectively) acquisitions were repeated on the Digirad X-ACT® camera with the patient sitting upright. There is partial resolution of the fixed inferior defect, indicating that with supine SPECT it was at least in part attributable to diaphragmatic attenuation. With additional AC (*third* and *fourth rows*) there is complete resolution of the inferior defect, indicating that with supine SPECT it was entirely attributable to diaphragmatic attenuation. There is also partial resolution of the resting apical defect, indicating some degree of stress-induced ischemia. Courtesy Gordon DePuey, St. Luke's-Roosevelt Hospital, New York, NY.

protocol with only 12.5 mCi and a 5-minute acquisition time using the new Discovery® camera, thereby significantly limiting patient radiation dose.

The very rapid imaging capability of the Discovery NM 530c® camera provides the opportunity for adjunctive techniques to potentially improve the diagnostic capabilities and accuracy of myocardial perfusion SPECT. Respiratory gating, which diminishes cardiac motion and potentially decreases diaphragmatic attenuation, thereby increasing diagnostic specificity, has been reported.[53] Buechel et al compared SPECT acquisitions triggered with breath-holding at deep inspiration to separate acquisitions acquired with x-ray AC but without breath-holding. Of 13 attenuation artifacts identified by AC, 4 (31%) were also partially unmasked by breath-holding. Pazhenkottil et al reported that by prolonging image acquisition time slightly to 5 minutes, gated image quality may be improved sufficiently to

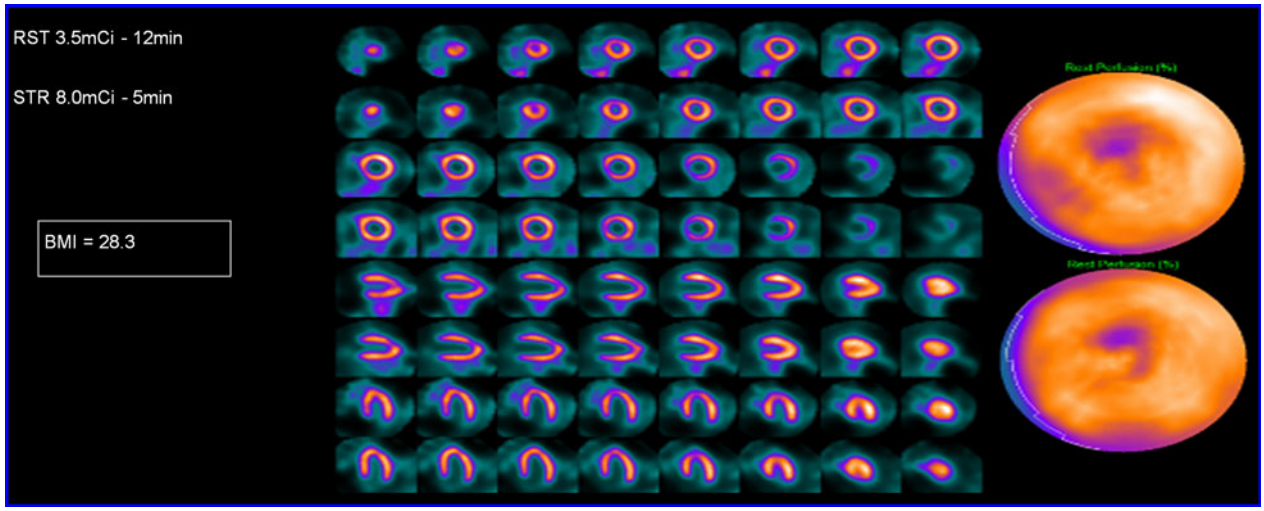

Figure 22. In this patient with a BMI of 28.3 a rest/stress SPECT scan was acquired on the D-SPECT® camera with significantly reduced Tc-99m sestamibi activity and image acquisition times. The patient received 3.5 mCi at rest and 8.0 mCi at stress. Acquisition times were 12 and 5 minutes, respectively. Image quality is excellent despite the reduced injected activity and scan acquisition times. Courtesy Spectrum Dynamics.

evaluate left ventricular dyssynchrony.[54] These investigators compared histogram bandwidth determined by phase analysis (Emory Toolbox®) of resting gated myocardial perfusion SPECT in 46 patients undergoing 15-minute SPECT on a standard dual-head NaI detector camera and 5-minute SPECT on the Discovery® camera and found no significant differences or the results obtained by the two methods. Hybrid imaging with x-ray CT, available with the Discovery® camera, allows for AC and image fusion with CT coronary angiography.[55,56]

ON THE HORIZON

Simultaneous Dual-Isotope SPECT

As described above, CZT solid-state detectors provide improved energy resolution as compared to NaI detectors. With improved discrimination of the photopeaks of Tc-99m and I-123, there is considerable future potential for simultaneous imaging of the radiopharmaceuticals labeled with these two isotopes. Similarly, Tl-201 emissions are better discriminated from Tc-99m photons using CZT detectors. Using the D-SPECT® camera, Berman et al[57] implemented a 20-minute sequential stress Tl-201/resting Tc-99m protocol, demonstrating similar image quality to that obtained using a standard rest/stress Tc-99m protocol. The advantage of using Tl-201 for stress imaging is its higher myocardial extraction, potentially allowing improved detection of stress-induced myocardial perfusion defects. Ben Haim et al[58] performed simultaneous 2.0 mCi resting Tl-201/6.8 mCi stress Tc-99m dual-isotope SPECT using the D-SPECT® camera in 27 consecutive patients and reported that image quality, diagnostic results, and SSS and SRS that were closely correlated with those obtained using a separate rest Tl-201/stress Tc-99m protocol in the same patients. Data were processed using a spill-over and scatter correction method, presumably minimizing the ''hole-tailing'' effect described above (Figure 24).

First-Pass Imaging and Evaluation of Coronary Flow Reserve

With high count-rate capabilities and list-mode acquisition the new CZT solid-state cameras provide the capability of performing high-quality first-pass radionuclide ventriculography.[37] Right ventricular function can be more accurately evaluated with first-pass imaging as compared to either planar equilibrium radionuclide ventriculography (MUGA) or gated myocardial perfusion SPECT. Assessment of left ventricular function during peak pharmacologic stress with either dobutamine or coronary vasodilators may be possible at the time of radiopharmaceutical injection. The adjunctive evaluation of left ventricular function at peak stress and at rest in conjunction with myocardial perfusion SPECT may increase diagnostic sensitivity and specificity of the latter.

An even more tantalizing potential capability is the assessment of coronary flow reserve.[8] Myocardial uptake of radiotracer is determined at stress and during peak pharmacologic coronary vasodilatation. It is now

possible to assess coronary flow reserve by this means using N-13 ammonia or Rb-82 PET. Quantification of coronary flow reserve has been demonstrated to provide adjunctive, prognostic value to myocardial perfusion PET.[59] The sensitivity of myocardial perfusion imaging is improved by the capability of detecting ''balanced'' ischemia, i.e., an equivalent, absolute decrease in myocardial perfusion in all vascular territories. Count-rate capabilities with the new solid-state detectors are now adequate to determine time-activity curves from the left ventricular cavity (input function) and from the myocardium (output function). Myocardial uptake is determined from these data using a two-compartment model, and a regional coronary flow reserve index is calculated as the ratio between myocardial uptake at stress versus rest. Although this technique has not yet been validated for SPECT systems, it seems promising. However, as compared to PET, SPECT methodology may be limited by the blunted myocardial extraction of Tc-99m sestamibi and tetrofosmin at high coronary flow rates. Moreover, to determine absolute myocardial blood flow AC, currently only available as an option on the Digirad X-ACT® and General Electric Discovery NM 530c® camera, is required.

Stress-Only Imaging

Stress-only myocardial perfusion SPECT has been demonstrated to be a practicable protocol in patients with no prior history of myocardial infarction and a relatively low pre-test likelihood of coronary artery disease. A normal stress-only scan confers the same favorable prognosis as a normal scan acquired using a conventional rest/stress protocol.[60] Stress myocardial perfusion SPECT with only a 5 mCi Tc-99m dose and a 12-16-minute acquisition time using a conventional dual-head NaI detector camera has been recently reported to be feasible in non-obese patients (Figure 25).[61] Apart from reducing the patient's time in the imaging laboratory and increasing laboratory efficiency by eliminating the resting scan, this protocol significantly decreases patient radiation exposure. Using the new software and hardware methods described above, which provide excellent image quality despite lower myocardial SPECT counting statistics in combination with a stress-only protocol, an even further reduction in patient radiation dose is feasible.

AC has been demonstrated to allow physicians to increase their confidence in interpreting stress-only studies as definitely normal or definitely abnormal and to reduce the need for resting imaging.[62] In a multicenter trial of 110 patients, Bateman et al[63] compared ''full-time'' myocardial perfusion SPECT acquired on a conventional dual-head NaI detector camera processed with FBP to scans ''stripped'' of data to produce ''half-time'' scans, which underwent Gd-153 line-source AC and were then processed with Astonish® reduced-time software. These investigators demonstrated improved image quality, diagnostic certainty, diagnostic sensitivity, and diagnostic specificity using this advanced software processing method in conjunction with AC. Moreover, perfusion defect SSSs and gated LVEFs were similar using the ''full-time'' and attenuation corrected ''half-time'' methods. Therefore, it seems that a combination of new software and hardware methods that cope with lower counting statistics and AC is optimal for stress-only imaging both to decrease patient radiation dose and to improve diagnostic confidence and accuracy.

CONCLUSIONS AND COMMENTARY

The new software and hardware methods described above have been convincingly demonstrated to decrease SPECT acquisition time, injected radioactivity, or both. The potential advantages of shortening image acquisition time are considerable. Patient tolerance is improved, the opportunity for patient motion is decreased, and laboratory throughput is improved. Decreasing radiopharmaceutical doses while maintaining a longer acquisition time to decrease patient radiation exposure effectively addresses concerns of the public and the media and the latest recommendations by the American Society of Nuclear Cardiology. Combining these two potential advantages, there is the opportunity to ''customize'' scan protocols to meet specific patient requirements. For example, in a younger patient in whom radiation exposure is a concern, a reduced radiopharmaceutical dose and a relatively longer acquisition may be preferable. In an elderly, arthritic, or uncooperative patient unable to tolerate a 12-15-minute SPECT acquisition, a full radiopharmaceutical dose and reduced-time SPECT acquisition would be beneficial. In an obese patient, in order to increase image counting statistics, as an alternative to ''weight-based'' (e.g., increased) radiopharmaceutical doses, a standard or reduced dose could be given in combination with a ''full-time'' or even prolonged SPECT acquisition with an image acquisition time customized to provide adequate counting statistics.

Although reduced image acquisition time and/or decreased radiopharmaceutical dose(s) are obvious potential clinical advantages of the software and hardware methods described above, these method also may potentially hold promise in improving the diagnostic capabilities of myocardial perfusion SPECT due to their ability to cope with lower image counting statistics. For example, investigators have already reported improvement in image quality by adding respiratory gating.[53]

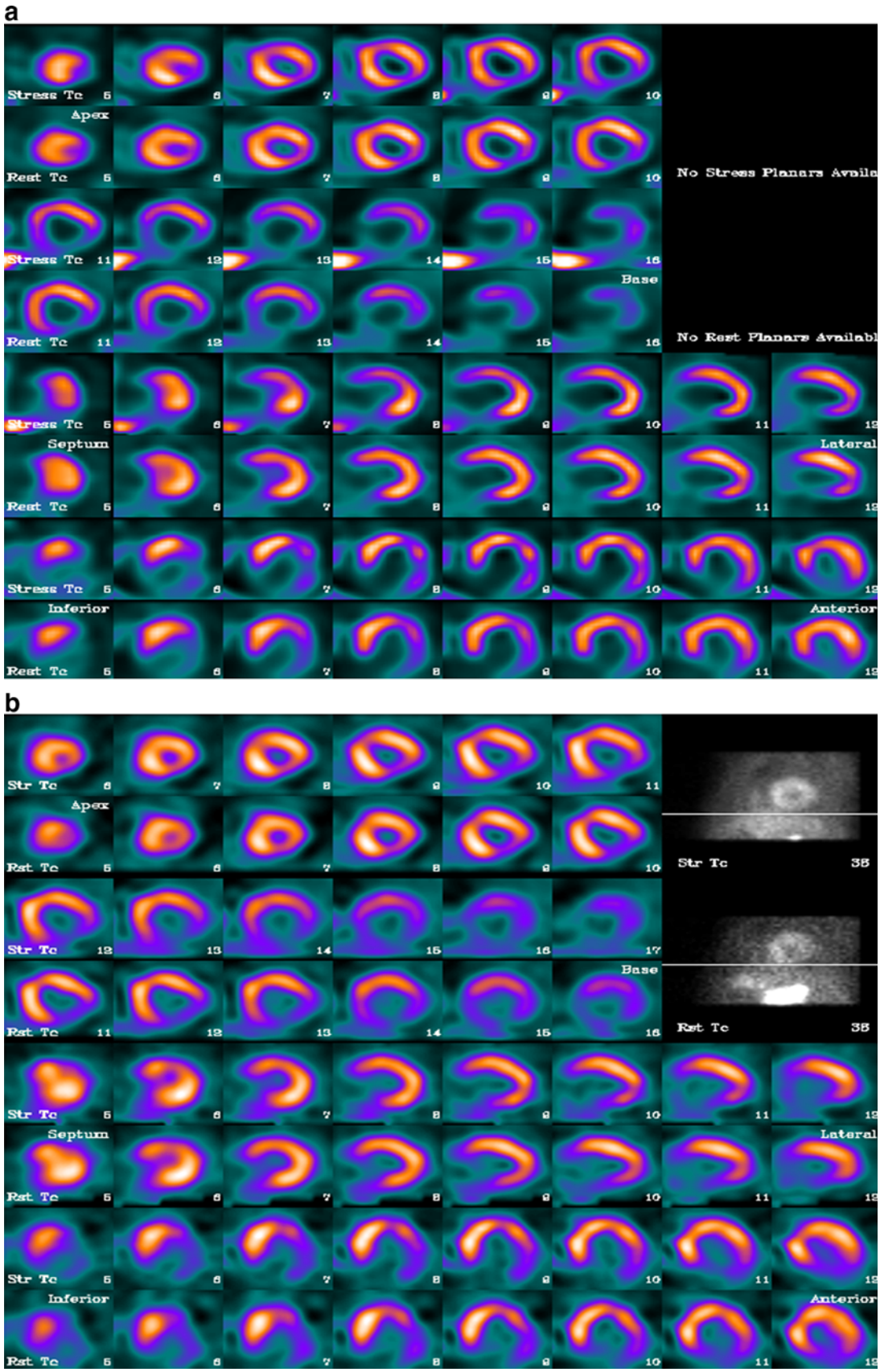
a
Stress Tc
Apex
Rest Tc
No Stress Planars Availa
Stress Tc
Base
Rest Tc
No Rest Planars Availabl
Stress Tc
Septum
Rest Tc
Lateral
Stress Tc
Inferior
Rest Tc
Anterior
b
Str Tc
Apex
Rst Tc
Str Tc 38
Str Tc
Base
Rst Tc
Rst Tc 38
Str Tc
Septum
Rst Tc
Lateral
Str Tc
Inferior
Rst Tc
Anterior

◀**Figure 23. A** Stress and rest standard-dose Tc-99m sestamibi myocardial perfusion SPECT was acquired on a conventional dual-detector NaI camera. SPECT acquisition times were 12 and 14 minutes, respectively. A severe and extensive fixed inferolateral perfusion defect is present. **B** Images were each reacquired on the Discovery NM 530c® camera with markedly reduced acquisition times: 2 and 4 minutes, respectively. Image quality is equivalent to that with the ''full-time'' conventional camera acquisition. Courtesy Ernest Garcia, Emory University, Atlanta, GA.

However, these potential capabilities to increase diagnostic accuracy should be explored much more fully. For example, it is very likely possible to increase the number of gated frames per cardiac cycle from 8 or 16 to $\geq$24, thereby providing both a more accurate ejection fraction and the potential for accurate quantitative analysis of systolic emptying and diastolic filling (i.e., peak systolic emptying rate and peak diastolic filling rate). Also, it would be highly desirable to ''freeze''

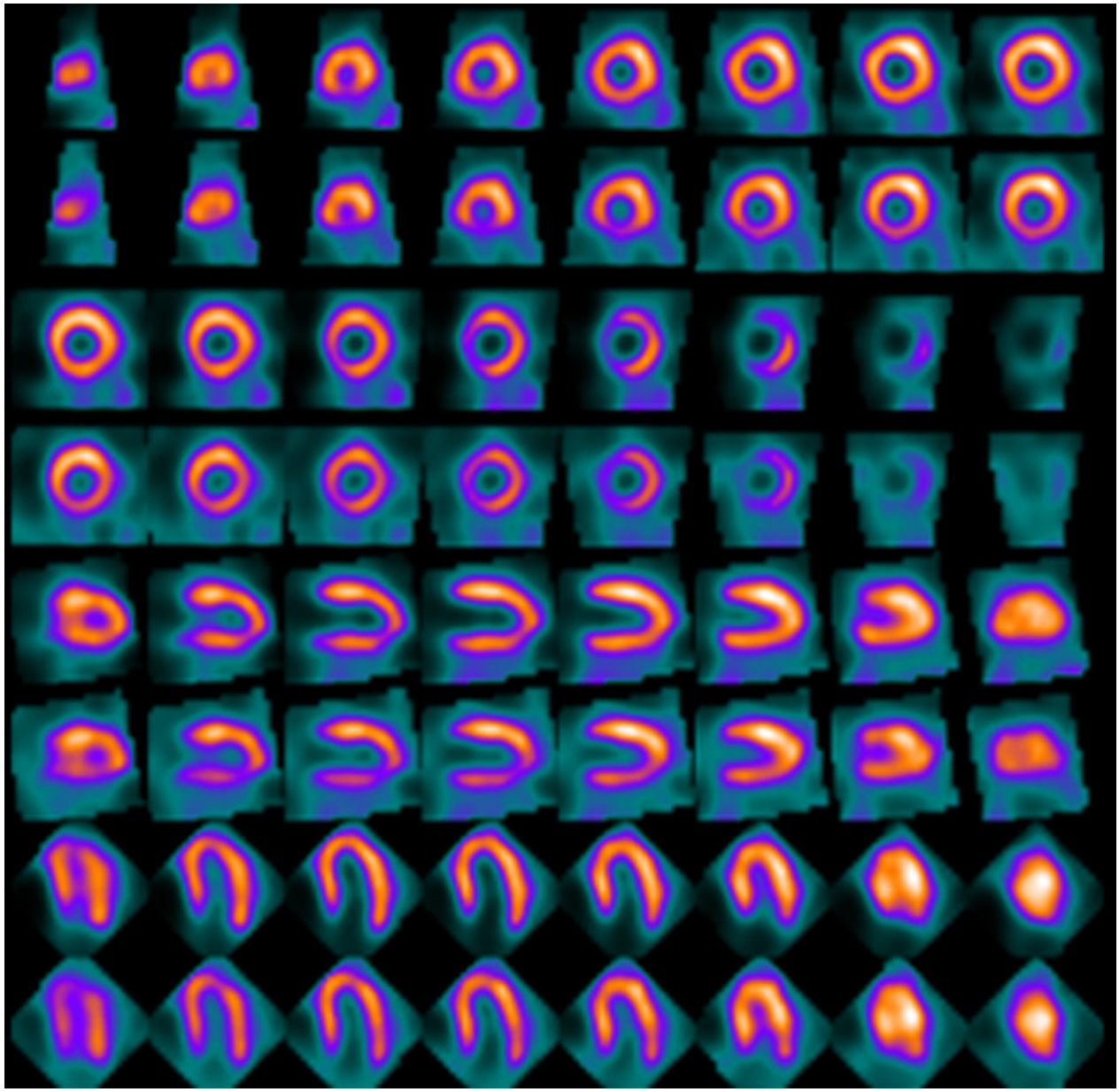

Figure 24. Simultaneous 2.0 mCi resting Tl-201/7.0 mCi stress Tc-99m sestamibi dual-isotope myocardial perfusion SPECT using the D-SPECT® CZT solid-state dedicated cardiac camera. Data were processed using a spill-over and scatter correction method.[58] Courtesy Spectrum Dynamics.

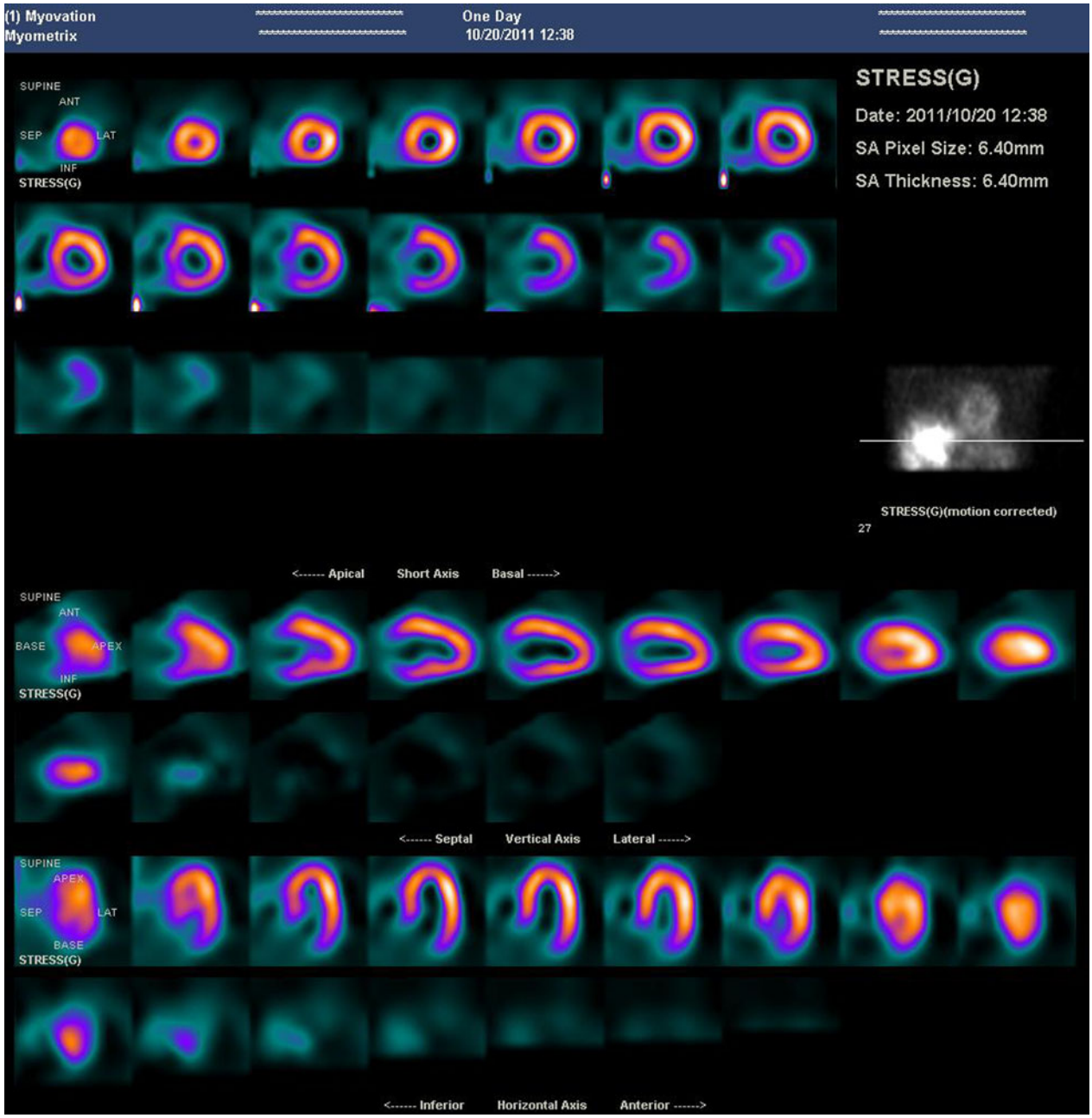

Figure 25. Stress-only myocardial perfusion SPECT was performed using a conventional dual-head NaI detector camera and only a 5 mCi Tc-99m sestamibi dose and a 16-minute acquisition time in this male patient with a 43″ chest circumference. Images were reconstructed using WBR Xpress3® ''quarter-time'' software. Because the SPECT images were unequivocally normal, a subsequent resting scan was unnecessary, thereby markedly decreasing patient radiation exposure. Courtesy Gordon DePuey, St. Luke's-Roosevelt Hospital, New York, NY.

cardiac motion by means of summing only end-diastolic gated frames in the summed perfusion tomograms, as describe more than a decade ago by Taillefer et al[64] to increase diagnostic sensitivity in detecting perfusion abnormalities. However, heretofore such techniques have not been practical because they significantly decrease image counting statistics and thereby introduce noise and potential artifacts. For example, the diagnostic accuracy of end-diastolic imaging was confounded by more marked soft tissue attenuation artifacts. However, now by combining advanced techniques that cope with lower counting statistics and AC, end-diastolic

''freeze-frame'' SPECT may be feasible. Other potential advantages of shorter acquisition times include the use of Tc-99m teboroxime, which is highly extracted by the myocardium but clears very rapidly, necessitating a rapid SPECT acquisition. There is also the possibility of performing gated SPECT acquisitions during dobutamine infusion to evaluate functional reserve as well as viability in a manner similar to that which is routinely accomplished with stress echocardiography. These applications most likely require SPECT acquisition times <5 minutes and list-mode acquisition, which are now clearly practical using a variety of the technical advancements described above.

If indeed the technical advancements reviewed in this article prove not only to decrease SPECT acquisition time and decrease radiation exposure but also to improve diagnostic accuracy in the detection of coronary artery disease, the Nuclear Cardiology community may be faced with the daunting task of reevaluating the diagnostic accuracy and prognostic value of myocardial perfusion SPECT. Such research would likely entail a prospective trial or trials with coronary angiographic correlation and extensive patient follow-up. Clearly, such an endeavor is too comprehensive and expensive to be undertaken by only one group of investigators or one instrumentation or software vendor. Such an effort will require sponsorship by national organizations and probably the Federal Government. However, if funding and sponsorship were available, before embracing this potential opportunity we should ask ourselves ''Is now the time?'' Are there radiopharmaceuticals on the horizon more highly extracted by the myocardium that will increase diagnostic accuracy? Do we anticipate further advancements in SPECT or PET technology that are worth waiting for? In the meantime, though, we should certainly embrace, tout, and clinically implement the remarkable myocardial perfusion SPECT technical advancements described above.

References

1. Einstein AJ, Moser KW, Thompson RC, Cerqueira MD, Henzlova MJ. Radiation dose from cardiac diagnostic imaging. Circulation 2007;116:1290-305.
2. Bogdanich W, Ruiz RR. FDA to increase oversight of medical radiation. New York Times, February 10, 2010;B7.
3. DePuey EG, Mahmarian JJ, Miller TD, Einstein AJ, Hansen CL, Holly TA, et al. Patient-centered imaging, ASNC Preferred Practice Statement. J Nucl Cardiol (in press).
4. Cerqueira MD, Allman KC, Ficaro EP, Hansen CL, Nichols KJ, Thompson RC, et al. Recommendations for reducing radiation exposure in myocardial perfusion imaging. J Nucl Cardiol 2010;17:709–18.
5. Patton JA, Slomka PJ, Germano G, Berman DS. Recent technological advances in nuclear cardiology. J Nucl Cardiol 2007;14: 501-13.
6. Garcia EV, Faber TL. New trends in camera and software technology in nuclear cardiology. Cardiol Clin 2009;27:227-36.
7. DePuey EG. New software methods to cope with reduced counting statistics: Shorter SPECT acquisitions and many more possibilities. J Nucl Cardiol 2009;16:335-8.
8. Sharir T, Slomka PJ, Berman DS. Solid-state SPECT technology: Fast and furious. J Nucl Cardiol 2010;17:890-6.
9. Garcia EV, Faber TL, Esteves FP. Cardiac dedicated ultrafast SPECT cameras: New designs and clinical implications. J Nucl Med 2011;52:210-7.
10. Metz CE. The geometric transfer function component for scintillation camera collimators with straight parallel holes. Phys Med Biol 1980;25:1059-70.
11. Tsui BMW, Gullberg GT. The geometric transfer-function for cone and fan beam collimators. Phys Med Biol 1990;35:81-93.
12. Tsui BMW, Hu HB, Gillard DR, Gullberg GT. Implementation of simultaneous attenuation and detector response correction in SPECT. IEEE Trans Nucl Sci 1988;35:778-83.
13. Tsui BMW, Frey EC, Zhao X, Lalush DS, Johnston RE, McCartney WH. The importance and implementation of accurate three-dimensional compensation methods for quantitative SPECT. Phys Med Biol 1994;39:509-30.
14. Tsui BMW, Zhao XD, Frey EC, Gullberg GT. Characteristics of reconstructed point response in three-dimensional spatially variant detector response compensation in SPECT. In: Grangeat P, Amans J-L, editors. Three-dimensional image reconstruction in radiology and nuclear medicine. Dordrecht: Kluwer Academic Publishers; 1996. p. 509-30.
15. Borges-Neto S, Pagnanelli RA, Shaw LK, Honeycutt E, Shwartz SC, Adams GL, et al. Clinical results of a novel wide beam reconstruction method for shortenings can time of Tc-99m cardiac SPECT perfusion studies. J Nucl Cardiol 2007;14:555-65.
16. DePuey EG, Gadiraju R, Clark J, Thompson L, Anstett F, Shwartz SC. Ordered subset expectation that maximization and wide beam reconstruction ''half-time'' gated myocardial perfusion SPECT functional imaging: A comparison to ''full-time'' filtered backprojection. J Nucl Cardiol 2008;15:547-63.
17. Philipe P, Bruyant J. Analytic and iterative reconstruction algorithms in SPECT. J Nucl Med 2002;43:1343-58.
18. Green PJ. Bayesian reconstruction from emission tomography data using a modified EM algorithm. IEEE Trans Med Imaging 1990;9:84-93.
19. Alenius S, Ruotsalainen U. Bayesian image reconstruction for emission tomography based on medium root prior. Eur J Nul Med 1997;24:258-65.
20. Farkash G, Kenig K, Grabnic M, Yuzefovich B, Sachs J, Bocher M. Volumetric quantitation of left ventricular perfusion and function from myocardial perfusion SPECT: Validation of a new algorithm [abstract]. J Nucl Cardiol 2006;13:S5.
21. Chen J, Garcia EV, Folks RD, Cooke CD, Faber TL, Tauxe L, et al. Onset of left ventricular mechanical contraction as determined by phase analysis of ECG-gated myocardial perfusion SPECT imaging: Development of a diagnostic tool for assessment of cardiac mechanical dyssynchrony. J Nucl Cardiol 2005;12:687-95.
22. Henneman MM, Chen J, Ypenburg C, Dibbets P, Bleeker GB, Boersma E, et al. Phase analysis of gated myocardial perfusion single-photon emission computed tomography compared with tissue Doppler imaging for the assessment of left ventricular dyssynchrony. J Am Coll Cardiol 2007;49:1708-14.
23. Henneman MM, Chen J, Dibbets-Schneider P, Stokkel MP, Bleeker GB, Ypenburg C, et al. Can LV dyssynchrony as assessed with phase analysis on gated myocardial perfusion SPECT predict response to CRT? J Nucl Med 2007;48:1104-11.

24. Heydari B, Jerosch-Herold M, Kwong R. Imaging for planning of cardiac resynchronization therapy. J Am Coll Cardiovasc Imaging 2012;5:93-110.
25. Liu YH, Lam PT, Sinusas AJ, Wackers FJT. Different effect of 180° and 360° acquisition orbits on the accuracy of SPECT imaging: Quantitative evaluation of phantoms. J Nucl Med 2002;43:1115-24.
26. Abufadel A, Eisner RL, Schafer RW. Differences due to collimator blurring in cardiac images with use of circular and elliptical orbits. J Nucl Cardiol 2001;8:458-65.
27. Bai C, Conwell R, Kindem J, Babla H, Gurley M, De Los Santos R, et al. Phantom evaluation of a cardiac SPECT/VCT system that uses a common set of solid-state detectors for both emission and transmission scans. J Nucl Cardiol 2010;17:459-69.
28. Vija AH, Malmin R, Yahil A, Zeintl J, Bhattacharya M, Rempel TD, et al. A method for improving the efficiency of myocardial perfusion imaging using conventional SPECT and SPECT/CT imaging systems. Hoffman Estates: Molecular Imaging, Siemens Medical Solution USA, Inc; 2010.
29. Rajaram R, Bhattacharya M, Ding X, Malmin R, Rempel TD, Vija H, et al. Tomographic performance characteristics of the IQ-SPECT system. Hoffman Estates: Molecular Imaging, Siemens Medical Solution USA, Inc; 2011.
30. Zeintl J, Rempel TD, Bhattacharya M, Malmin RE, Vija AH. Performance characteristics of the SMARTZOOM® collimator. Hoffman Estates: Molecular Imaging, Siemens Medical Solution USA, Inc; 2011.
31. Corbett J, Meden J, Ficaro E. Clinical validation of attenuation corrected cardiac imaging with IQ-SPECT/CT [abstract]. J Nucl Med 2010;4:733.
32. Gambhir SS, Berman DS, Ziffer J, Nagler M, Sandler M, Patton J, et al. A novel high-sensitivity rapid-acquisition single-photon cardiac imaging camera. J Nucl Med 2009;50:635-43.
33. Esteves FP, Raggi P, Folks RD, Keidar Z, Askew W, Rispler S, et al. Novel solid-state-detector dedicated cardiac camera for fast myocardial perfusion imaging: Multicenter comparison with standard dual detector cameras. J Nucl Cardiol 2009;16:927-34.
34. Blevis I, Tsukerman L, Volokh L, Hugg J, Jansen F, Bouhnik JP. CZT gamma camera with pinhole collimator: Spectral measurements. In 2008 IEEE nuclear science symposium conference record. ISBN: 978-1-4244-2715-4/08.
35. Erlandsson K, Kacperski K, Van Gramberg D, Hutton B. Performance evaluation of D-SPECT: A novel dedicated cardiac SPECT scanner. Phys Med Biol 2009;54:2635-49.
36. Hutton B, Erlandsson K, Kacperski K, Van Gramberg D, Roth N. Performance evaluation of D-SPCT—a novel dedicated cardiac SPECT scanner. J Nucl Med 2008;49:124P.
37. Bocher M, Blevis IM, Tsukerman L, Shrem Y, Kovalski G, Volokh L. A fast cardiac gamma camera with dynamic SPECT capabilities: Design, system validation and future potential. Eur J Nucl Med Mol Imaging 2010;37:1887–902.
38. Gambhir SS, Berman DS, Ziffer J, Nagler M, Sandler M, Patton J, et al. A novel high-sensitivity rapid-acquisition single-photon cardiac imaging camera. J Nucl Med 2009;50:635-43 (On line supplemental material).
39. Hillel I, Hanney M, Redgate S, Taylor J, Randall D. Assessing the performance of a solid-state cardiac gamma camera prior to its introduction into routine clinical service. J Nucl Med 2011;52:1937.
40. Basso D, Passmore G, Holman M, Rogers W, Walters L, Zecchin T, et al. Semiqualitative visual and quantitative morphometric evaluations of reduced scan time and wide-beam reconstruction in rest-gated stress SPECT myocardial perfusion imaging. J Nucl Med Technol 2009;37:233-9.
41. Marcassa C, Campini R, Zoccarato O, Calza P. Wide beam reconstruction for half-dose or half-time cardiac gated SPECT acquisitions: Optimization of resources and reduction in radiation exposure. Eur J Nucl Med 2010;38:499-508.
42. Druz R, Phillips L, Chugkowski M, Boutis L, Rutkin B, Katz B. Wide-beam reconstruction half-time SPECT improves diagnostic certainty and preserves normalcy and accuracy: A quantitative perfusion analysis. J Nucl Cardiol 2011;18:52-61.
43. Venero CV, Heller GV, Bateman TM, McGhie AI, Ahlberg AW, Katten D, et al. A multicenter evaluation of a new post-processing method with depth-dependent collimator resolution applied to full-time and half-time acquisitions without and with simultaneously acquired attenuation correction. J Nucl Cardiol 2009;16:714-25.
44. Cullom SJ, Saha K, Heller GV, Bateman TV. An optimized iterative reconstruction and processing protocol for ''half-time'' (32 projections) REST/STRESS Tc99m-sestamibi myocardial perfusion SPECT. J Nucl Cardiol 2008;15:S6.
45. DePuey EG, Bommireddipalli S, Clark J, Thompson L, Srour Y. Wide beam reconstruction ''quarter-time'' gated myocardial perfusion SPECT functional imaging: A comparison to ''full-time'' ordered subset expectation maximum. J Nucl Cardiol 2009;16:736-52.
46. DePuey EG, Bommireddipalli S, Clark J, Leykekhman A, Thompson LB, Friedman M. A comparison of the image quality of full-time myocardial perfusion SPECT versus wide beam reconstruction half-time and half-dose SPECT. J Nucl Cardiol 2011;18:273-80.
47. Maddahi J, Mendez R, Mahmarian J, Thomas G, Bai C, Babla H, et al. Prospective multi-center evaluation of rapid gated SPECT myocardial perfusion and upright imaging. J Nucl Cardiol 2009;16:351-7.
48. Sharir T, Ben-Haim S, Merzon K, Prochorov V, Dickman D, Ben-Haim S, et al. High-speed myocardial perfusion imaging: Initial clinical comparison with conventional dual detector anger camera imaging. J Am Coll Cardiol Imaging 2008;1:156-63.
49. Sharir T, Slomka PJ, Hayes SW, DiCarli MF, Ziffer JA, Martin WH, et al. Multicenter trial of high-speed versus conventional single-photon emission computed tomography imaging: Quantitative of myocardial perfusion and left ventricular function. J Am Coll Cardiol 2010;55:1965-74.
50. Buechel RR, Herzog BA, Husmann L, et al. Ultrafast nuclear myocardial perfusion imaging on a new gamma camera with semiconductor detector technique: First clinical validation. Eur J Nucl Med Mol Imaging 2010;37:773-8.
51. Herzog BA, Buechel RR, Katz R, et al. Nuclear myocardial perfusion imaging with a cadmium-zinc-telluride detector technique; optimized protocol for scan time reduction. J Nucl Med 2010;51:46-51.
52. Duvall WL, Croft LB, Godiwala T, Ginsberg E, George T, Henzlova MJ. Reduced isotope dose with rapid SPECT MPI imaging: Initial experience with a CZT SPECT camera. J Nucl Cardiol 2010;17:1009-14.
53. Buechel RR, Pazhenkottil AP, Herzog BA, et al. Real-time breath-hold triggering of myocardial perfusion imaging with a novel cadmium-zinc-telluride detector gamma camera. Eur J Nucl Med Mol Imaging 2010;37:1903-8.
54. Pazhenkottil AP, Buechel RR, Herzog BA, et al. Ultrafast assessment of left ventricular dyssynchrony from nuclear myocardial perfusion imaging on a new high-speed gamma camera. Eur J Nucl Med Mol Imaging 2010;37:2086-92.
55. Herzog BA, Buechel RR, Husmann L, et al. Validation of CT attenuation correction for high-speed myocardial perfusion imaging using a novel cadmium-zinc-telluride detector technique. J Nucl Med 2010;51:1539-44.

56. Pazhenkottil AP, Husmann L, Kaufmann PA. Cardiac hybrid imaging with high-speed single-photon emission computed tomography/CT camera to detect ischemia and coronary artery obstruction. Heart 2010;96:2050.
57. Berman DS, Kang X, Tamarappoo B, Wolak A, Hayes SW, Nakazato R, et al. Stress thallium-201/rest technetium-99m sequential dual isotope high-speed myocardial perfusion imaging. JACC Cardivasc Imaging 2009;2:273-82.
58. Ben-Haim S, Kacperski K, Hain S, Van Gramberg D, Hutton BF, Erlandsson K, et al. Simultaneous dual-radionuclide myocardial perfusion imaging with a solid-state dedicated cardiac camera. Eur J Nucl Med Mol Imaging 2010;37:1710-21.
59. Herzog BA, Husmann L, Valenta I, Gaemperli O, Siegrist PT, Tay FM, et al. Long-term prognostic value of 13N-ammonia myocardial perfusion positron emission tomography added value of coronary flow reserve. J Am Coll Cardiol 2009;54:150-6.
60. Chang SM, Nabi F, Xu J, Raza U, Mahmarian JJ. Normal stress-only versus standard stress/rest myocardial perfusion imaging. J Am Coll Cardiol 2010;55:221-30.
61. DePuey G, Ata P, Wray R. 5 mCi stress myocardial perfusion SPECT with a conventional NaI camera [abstract]. J Nucl Med (submitted).
62. Heller GV, Bateman TM, Johnson LL, Cullom SJ, Case JA, Galt JR, et al. Clinical value of attenuation correction in stress-only Tc-99m sestamibi SPECT imaging. J Nucl Cardiol 2004;11:273-81.
63. Bateman TM, Heller GV, McGhie AI, Courter SA, Golub RA, Case JA, et al. Multicenter investigation comparing a highly efficient half-time stress-only attenuation correction approach against standard rest-stress Tc-99m SPECT imaging. J Nucl Cardiol 2009;16:726-35.
64. Taillefer R, DePuey EG, Udelson JE, Beller GA, Benjamin C, Gagnon A. Comparison between the end-diastolic images and the summed images of 99m-Tc sestamibi gated SPECT perfusion study in detection of coronary artery disease in women. J Nucl Cardiol 1999;6:169-76.